# NATIONAL ADVISORY COMMITTEE FOR AERONAUTICS

**TECHNICAL NOTE 2385**

# FUNDAMENTAL AGING EFFECTS INFLUENCING HIGH-TEMPERATURE PROPERTIES OF SOLUTION-TREATED INCONEL X

By D. N. Frey, J. W. Freeman, and A. E. White

University of Michigan


Washington
June 1951

NATIONAL ADVISORY COMMITTEE FOR AERONAUTICS

TECHNICAL NOTE 2385

# FUNDAMENTAL AGING EFFECTS INFLUENCING HIGH-TEMPERATURE PROPERTIES OF SOLUTION-TREATED INCONEL X

By D. N. Frey, J. W. Freeman, and A. E. White

## SUMMARY

Studies were made of the effects of various aging treatments on the mechanical properties of solution-treated Inconel X at 1200° and 1500° F for rupture times of 0.1 to 1000 hours. Specimens were aged at 1200°, 1400°, and 1600° F for time periods up to 1000 hours. Microstructure analyses of the aged specimens were made by means of X-ray diffraction studies and optical- and electron-micrographic examinations.

Correlations of the mechanical properties with the structural analyses were made with the aid in part of mathematical analyses. From these correlations and by comparison with previous work on low-carbon N-155 alloy, two classes of austenitic alloys subject to precipitation from supersaturated solid solution were established. In one class (i.e., low-carbon N-155 alloy), no beneficial effect from precipitation, as far as creep resistance is concerned, could be produced by aging. This was due to excessive spacing between precipitate particles and depletion of the matrix of the large "incongruous" atoms forming the precipitate. In the other class (i.e., Inconel X), considerable improvement in creep resistance from precipitation was found at low temperatures (1200° F) because the precipitate was formed in a certain "critical dispersion." For this critical dispersion, agreement was found with an extension of the rate theory of creep which relates logarithmic creep rate linearly to internal stress resulting from the precipitation. At higher temperatures (1500° F), behavior similar in nature to that of the first class was found, inasmuch as precipitate particle spacing either was initially or rapidly became too large.

In both classes, aging resulted in some improvement in rupture strength in the range from 100- to 1000-hours rupture time at low temperatures (1200° F). Detailed analysis of the data showed improvement was obtained in low-carbon N-155 apparently through formation of a grain boundary phase and in Inconel X through increasing the resistance to creep prior to fracture.

## INTRODUCTION

This report concerns fundamental studies that have been made of the mechanisms by which aging treatments influence the mechanical properties of Inconel X alloy for time periods up to 1000 hours at temperatures of 1200° and 1500° F. These studies are part of a general investigation of the fundamental factors which control the properties of austenitic alloys having exceptionally high creep and rupture strengths in this temperature range. One previous report has been issued on an investigation of low-carbon N-155 alloy (reference 1) which is similar to that being reported herein for Inconel X.

Inconel X alloy was selected for investigation in order to obtain information on an alloy with marked precipitation-hardening characteristics in contrast with low-carbon N-155 which age-hardens only slightly, although subject to considerable precipitation during aging.

The nature of the structures produced by various aging treatments prior to testing has been established by X-ray analysis of the matrix materials and by both optical- and electron-micrographic examinations. Correlations of the results of the structural studies with the mechanical properties have been made. Comparisons with the previously determined aging effects on low-carbon N-155 alloy supplement these results.

This work was done under the sponsorship and with the financial assistance of the National Advisory Committee for Aeronautics as part of its program at the University of Michigan. The over-all purpose of the program is to establish the fundamental properties of high-temperature alloys in order to make efficient use of alloy content, to produce uniform and known properties in any given alloy, and to develop still better materials for aircraft propulsion service.

## MATERIALS TESTED

Hot-rolled, 1-inch, round bar stock from Inconel X melt number Y3724-X was used. The reported chemical composition for this melt was as follows:

| | C | Mn | Fe | S | Si | Cu | Ni | Cr | Al | Ti | Cb |
|---|---|---|---|---|---|---|---|---|---|---|---|
| Weight percent | 0.04 | 0.56 | 6.59 | 0.007 | 0.38 | 0.03 | 73.22 | 14.97 | 0.78 | 2.38 | 1.02 |
| Atomic percent | .19 | .56 | 6.65 | ----- | .76 | .03 | 70.35 | 16.19 | 1.63 | 2.80 | .56 |

The reported fabrication schedule is given in the appendix. The position of the bars used relative to the original ingot was unknown. Figure 1 shows the microstructure of this bar stock as received.

## EXPERIMENTAL PROCEDURE

### Heat Treatment

As a preliminary, an investigation of the grain-coarsening characteristics and solution of the precipitants of the as-rolled bar stock was carried out in a small globar furnace as a function of solution temperature and, to a lesser extent, of solution time. From this investigation, a solution treatment of 4 hours at 2050° F followed by water-quenching was selected. This treatment was found to give the most effective solution of excess constituents while avoiding excessive grain sizes for the X-ray investigations. Figure 2 shows the microstructure after solution treatment.

Enough bar stock for all the mechanical test specimens and small slugs for X-ray analysis and micrographic examination were then solution-treated in a gas-fired furnace. After completion of solution treatment, the specimens were given the desired aging treatments in small electric-resistance furnaces with a still air atmosphere. Three aging temperatures were used, 1200°, 1400°, and 1600° F, with aging times of 1, 10, 100, and 1000 hours at each of the three temperatures.

### Structural Analysis

The structural analysis was carried out on small slugs heat-treated along with the mechanical test specimens. In general, five kinds of tests were carried out as part of the analysis: Hardness measurements, optical-micrographic examination, electron-micrographic examination, determination of X-ray diffraction-line widths, and determination of X-ray diffraction-line integrated intensities.

Hardness measurements were made with a Brinell testing unit using a 10-millimeter ball and a 3000-kilogram load. On any given sample, two impressions were made on a plane transverse to the rolling direction. Two diameters, at 90° to each other, were measured on each impression and the resulting four measurements were averaged.

For optical-micrographic examinations, surfaces were mechanically polished in a conventional manner and electrolytically etched with 10 percent oxalic acid. It was found that this etching frequently left a brown stain on the polished surface which was easily removed by

swabbing the surface with cotton dipped in 10 percent chromic acid. For electron-micrographic examination, Formvar replicas were made of the same surfaces used for optical examination. These replicas were shadow-cast with chromium or uranium and were examined and photographed in an RCA Model B electron microscope.

All X-ray examinations involved first the preparation of surfaces free from artificial strain. For a discussion of the electrolytic etching and polishing techniques involved, see reference 1. For Inconel X it was found necessary to remove electrolytically a minimum layer of metal 0.030 inch thick to insure such a strain-free surface. The glycerin and hydrochloric-acid electrolyte, as discussed in reference 1, was found to have a satisfactory efficiency. This electrolyte also gave satisfactory surfaces and was used for preparing Inconel X samples.

Determination of X-ray diffraction-line widths was carried out on the [220] line (back-reflection region) using the photographic method covered in reference 1. For determination of line intensities, a Norelco spectrometer was used. Because of the coarse grain size of the Inconel X stock, special integrating techniques had to be developed in order to achieve reproducible results. For this reason, the specimen mount shown in figure 3 was constructed for the spectrometer. The mount imparts two simultaneous motions to the plane surface exposed to the X-ray beam - a rotation at approximately 7 rps about an axis normal to and in the center of the irradiated plane and a translation normal to the axis of spin with a period of one second. The amplitude of the translation was fixed so that the X-ray beam effectively covered a circle on the irradiated surface 5/8 inch in diameter. With this arrangement, integrated intensities were measured with a mean deviation of approximately 10 percent. Integrated intensities, as a function of aging conditions, were chosen for study rather than peak intensities, as for the previous work on N-155 alloy (reference 1). For measurement of the areas of the Norelco spectrometer plots, a Keuffel and Esser No. 3010 planimeter was used. As a standard of comparison -200 mesh nickel powder, prepared in the form of a briquet with Duco cement, was used. This standard of comparison was chosen in order to have a material with about the same atomic scattering power and with diffraction maximums at approximately the same angles.

## Mechanical Properties

The mechanical test specimens, 0.250 inch in diameter, were treated and tested according to the schedule of table I.

Rupture tests were made at 1200° and 1500° F. For rupture times over 8 hours, the tests were conducted in a beam-loaded unit with a mechanical advantage of 23. For rupture times shorter than 8 hours, a

hydraulic tensile testing machine was used with the load maintained to ±400 psi, as read on the machine dial.

All creep tests were conducted in beam-loaded creep units equipped with modified Martens optical extensometers. For high creep rates, the least reading of the extensometer was $14.3 \times 10^{-6}$ inch per inch; for the tests at low creep rates, the least reading was $8.6 \times 10^{-6}$ inch per inch. Two stresses, 65,000 and 50,000 psi, were used for the creep tests at 1200° F. In most cases, 65,000 psi gave extremely fast rates while 50,000 psi gave rates approaching the minimum measurable. For similar reasons, the two creep test stresses chosen for 1500° F were 25,000 and 15,000 psi.

For determination of yield points at 1200° F, the creep unit loading curves were used, provided the creep stress was above the yield stress; if not, a short-time tensile test run in the hydraulic unit was used. Loading rates were comparable for both methods - approximately 1000 psi per second. Temperatures in all cases were measured with Chromel-Alumel thermocouples and were maintained within ±4° F of the desired temperature during the duration of the test.

## RESULTS AND DISCUSSION

### Structural Changes as a Result of Aging

Microstructures.- Examination of the microstructures of the various aged samples of Inconel X was carried out as part of the determination of structural changes resulting from aging; figures 4 to 9 show the results. Superiority of the electron micrographs, in regard to depth of field and resolution, is particularly marked when dealing with the finer precipitate particles. Nucleation and appearance of the precipitate at the various times and temperatures used seem normal for aging systems in general. There appears to be little grain boundary phase present in the samples aged for long time periods at either 1400° or 1600° F, although the series aged at 1200° F exhibits some sort of grain boundary phase after long aging (see fig. 7(b)). This latter series of samples also showed no precipitate particles, even after 1000 hours of aging. A lineal analysis of large areas of electron micrographs of the samples aged 1000 hours at 1400° and 1600° F showed 29 and 4 percent[1] precipitate by volume, respectively. The decrease in precipitate volume was ascribed to the increasing solubility of the precipitating phase with increasing temperature.

---

[1]The lineal analysis for this sample had a mean deviation of ±3 percent because of difficulty in obtaining a sufficient number of particles in the field of observation.

Hardness.- Hardness measurements, shown in figure 10, immediately point out the fact that maximum hardness of aged Inconel X samples examined in this investigation occurs when the precipitate is not visible, even at 10,000X using the techniques described previously. (Compare the hardnesses of samples aged 1000 hours at 1200° and 1400° F with their electron micrographs shown in figures 7(b) and 8(c), respectively.) This behavior is in marked contrast with that previously reported for low-carbon N-155. In that case, the maximum hardnesses observed coincided with the presence of visible precipitate, even in the optical micrographs at 1000X.

X-ray diffraction-line widths.- Figure 11 shows the results of the line width measurements made to evaluate the internal strains due to precipitation. The strains shown are relative to the material in the unaged or solution-treated state. The origin of these internal strains is assumed to be the misfit between precipitate and mother lattice. The disappearance of these strains is assumed to be due to the formation of an interface between the individual precipitates and the matrix. Both concepts have been investigated theoretically by Mott and Nabarro (see reference 2).

Comparison of the results of figure 11 with those of figure 10 shows a rather good correlation between hardness and internal strain. (This was also the case with low-carbon N-155 alloy.) Comparison of the internal strain measurements with the electron micrographs shows that the point of maximum internal strain was reached with no visible precipitate. This indicated that the size of the particles at this point must be below the resolving power of the electron microscope which was of the order of $2 \times 10^{-6}$ centimeter. Only a rough estimate of their spacing could be made. The spacing of the particles in material aged at 1400° F was of the order of $5 \times 10^{-5}$ centimeter. This spacing was approximately one order of magnitude less than the spacing at 1600° F. The particles at 1200° F could be expected to be spaced one order of magnitude less than at 1400° F or approximately $5 \times 10^{-6}$ centimeter apart. Particles with this spacing would be very difficult to distinguish from the rather pitted and rough background formed by the matrix.

It is also interesting to note that the maximum internal strain due to precipitation found in aged Inconel X was approximately four times that found in low-carbon N-155. However, as the following discussion points out, the important difference between the two alloys is the spacing between precipitate particles when internal strains are high.

X-ray diffraction-line integrated intensities.- Measurements were made of diffraction-line integrated intensities in an attempt to obtain still further information regarding structural changes occurring in solution-treated Inconel X during aging. Three effects of interest have been reported in the literature concerning the theory of intensities of X-ray diffraction lines in precipitating alloy systems.

(1) First, and rather obvious, is the fact that if one phase (the precipitating phase) is being formed at the expense of another (the matrix phase), the intensity of the diffraction lines of the latter phase will drop. Neglecting any extinction and microabsorption, the expression for the integrated intensity of the matrix lines in a precipitating polycrystalline system with the experimental setup used in this investigation is:

$$P_{[HKL]} = P_o \times \text{Constant} \times \frac{N^2}{\mu} \times \frac{1 + \cos^2 2\theta}{\sin 2\theta \sin \theta} \times F_{[HKL]}^2 \times j_{[HKL]} \times e^{-16\pi^2 \bar{u}^2 \left(\frac{\sin \theta}{\lambda}\right)^2} \quad (1)$$

where

$F_{[HKL]}$ crystal structure factor

$j_{[HKL]}$ multiplicity

$N$ number of unit cells per unit volume

$P_o$ power in primary beam

$P_{[HKL]}$ integrated intensity power of any diffraction line obtained from spectrometer plot

$\bar{u}^2$ mean square displacement due to heat motion, A

$\theta$ Bragg angle, degrees

$\lambda$ wave length of X-radiation used, centimeters

$\mu$ effective absorption coefficient

(2) Equation (1) is the intensity expression for the "ideally imperfect crystal" and is derived on the basis that the intensity of the primary X-ray beam at any given point of the crystal is unaffected by any diffraction that took place prior to reaching the given point. In perfect crystals, equation (1) is obviously wrong but as the crystals are made less perfect through such a mechanism as cold-work, the intensities approach equation (1).

Extinction corrections to equation (1) that allow for the energy extraction due to diffraction might be expected to vary with aging. They are of two types, primary and secondary. Primary extinction is the power loss due to diffraction within any one crystal; secondary extinction is the power loss due to diffraction in the crystals traversed by

the incident beam before it reaches a particular crystal. The latter type would appear in polycrystalline materials and not in a true single crystal. The theoretical determination of the form the corrections should take is far from complete. Evidence to date indicates that secondary extinction is negligible in systems with crystal particles smaller than $10^{-2}$ centimeter. Thus, this type of correction will be neglected in this report as the crystal particles certainly cannot be any bigger than $10^{-2}$ centimeter, as figure 2 shows. However, the crystal particles could be considerably smaller than this if each crystal in figure 2 was actually a mosaic composed of many crystallites. For primary extinction, the Darwin correction term (see reference 3) is a hyperbolic tangent function:

$$P'_{[HKL]} = P_{[HKL]} \frac{\tanh \left( \text{Constant} \times \frac{1}{\sin 2\theta} F_{[HKL]}^2 d^2 \cot \theta \right)^{\frac{1}{2}}}{\left( \text{Constant} \times \frac{1}{\sin 2\theta} F_{[HKL]}^2 d^2 \cot \theta \right)^{\frac{1}{2}}} \qquad (2)$$

where $d$ is the thickness of the ideal or perfect crystals which make up the aggregate (the mosaic). It is readily seen that the correction term approaches unity as $d$ approaches zero and that it also approaches zero as $\theta$ approaches zero. Thus, it is the lower order lines that are extinguished most by relatively large values of $d$.

Rejection from supersaturated solid solution of solute atoms might be assumed to be equivalent to converting the crystals of a polycrystalline material from imperfect ones to more perfect ones, thus increasing the magnitude of the extinction corrections. This effect would be the over-all one, with the possibility of the extinction correction being smallest at some intermediate step in aging. This step might coincide with the point of maximum internal strain due to precipitate misfit or to any other effect that would give a smaller mosaic size than that before or after the aging process. Thus, variation in the corrections leads to information regarding the internal structure of the alloy.

(3) The third item of importance is the apparent heat motion. Equation (1) contains a correction term for the heat motion of the lattice $e^{-2M}$ where $M$ equals $8\pi^2 \bar{u}^2 \left(\sin \theta/\lambda\right)^2$. It will be noted that this term decreases in magnitude with increasing $\theta$ which is opposite to the character of the extinction correction. Hengstenberg and Mark (see reference 4) obtained data from precipitation-hardened Duralumin which indicated that the precipitation process at maximum hardness introduced an additional correction term of the type $e^{-2M}$ This was called the "frozen heat motion." Presumably the displacement

represented by $\bar{u}^2$ was due to a very short-period disturbance from the precipitant nuclei, such displacement being an average over space and not so time dependent as the true heat motion.

In this investigation, integrated intensity values, as a function of $\theta$ over a limited $\theta$ range and with -200 mesh nickel powder as a standard of comparison, were obtained for solution-treated Inconel X in various aged conditions. The results are shown in figure 12. This investigation of line intensities should be considered preliminary in nature since only three lines ($[\bar{1}11]$, $[\bar{2}00]$, and $[\bar{2}20]$) were measured - the three lines in the range of the Norelco spectrometer.

For maximum value, the standard of comparison should satisfy equation (1). If it does, the theoretical ratio of intensities of Inconel X diffraction lines to any given line of the nickel standard may be calculated, neglecting extinction, density, or frozen-heat-motion corrections to the Inconel X values. From deviations from these ratios, extinction, density, and frozen-heat-motion corrections may be calculated for Inconel X. To check the usefulness of the standard nickel powder, the theoretical ratios of the intensities of the $[\bar{2}00]$ and $[\bar{2}20]$ nickel lines to the $[\bar{1}11]$ nickel line were calculated using equation (1).

Table II summarizes these calculations along with the observed ratios obtained from the Norelco spectrometer. It can be seen from this table that fair agreement was found within the limited range of $\theta$ used. Considering the uncertainties involved in the determinations of the theoretical and experimental values, it is concluded that the nickel powder is free from extinction and other possible intensity corrections. This is to be expected as the preparation of the nickel powder in itself should produce a nearly ideally imperfect crystal.

Next, the theoretical ratios of the $[\bar{1}11]$, $[\bar{2}00]$, and $[\bar{2}20]$ lines of Inconel X to the nickel $[\bar{1}11]$ lines were calculated, neglecting extinction and random atomic displacements. Equations of type (1) were used, taking due account of differences between the values of $\mu$, $N$, $F_{[\bar{H}K\bar{L}]}$, and so forth, for the nickel powder and Inconel X alloy in the form of polycrystalline bar stock. These calculations are summarized in table III, along with the observed ratios. (See also fig. 12.) It is apparent that in some cases extinction and random-atomic-displacement terms are of considerable magnitude.

Using the previously stated correction for these effects, values of d, the mosaic size, and $\bar{u}$, the "frozen" random atomic displacement, were calculated. Results of these calculations are shown in table IV.

To obtain approximately the aging time dependence of the changes of the constants d and $\bar{u}$ shown in table IV, values of the intensity of

the [111] line of Inconel X, expressed in terms of the value for the unaged (solution-treated) material, were taken. Figure 13 shows the results.

From figure 13 and the values of d and $\bar{u}$ of table IV, the following tentative conclusions can be drawn. These conclusions should be considered tentative until more lines, over a greater range of $\theta$, are investigated.

(1) Aging at 1200° F of solution-treated stock results in no appreciable change in the random-atomic-displacement value $\bar{u}$ when compared with that of unaged solution-treated material.

The relatively large value of $\bar{u}$ ($\pm$0.07 A) in unaged material is due to the presence of "incongruous" atoms or small groupings of them in random solid solution. Maintenance of this large value of $\bar{u}$ after aging at 1200° F could be due to the formation of precipitant nuclei, composed of only a few atoms, that give rise to strain centers of very short period.

(2) Aging for long time periods at 1400° F results in lowering of [111] line integrated intensities, primarily because of the formation of an additional phase. The higher order intensities are increased relatively because of reduction of $\bar{u}$ by rejection of precipitate atoms.

No detailed analysis of samples aged for shorter times at 1400° F was made. However, aging for short time periods (0 to 10 hr) at 1400° F most probably results in the same changes occurring at a slower rate at 1200° F.

The maximum ratio occurring between 10 and 100 hours on the 1400° F aging curve of figure 13 probably is due to further reduction in the already small mosaic size by formation of definite precipitate centers with smaller spacing than the mosaic size at 1200° F. The random atomic displacement is probably starting to decrease to the value obtained for the sample aged for 1000 hours at 1400° F. This decrease is due to the aforementioned rejection of the precipitant atoms from the matrix.

(3) Aging at 1600° F resulted in only 4 percent precipitation after 1000 hours at temperature. Thus, the decrease in intensity is due almost entirely to increase in mosaic size. As at 1400° F, the random atomic displacement was reduced to a very small value. This again is attributable to the rejection of the precipitate atoms from random solid solution. When cognizance is taken of the much smaller amount of precipitate formed at 1600° F (probably reflecting the slope of the solubility curve for the precipitate between 1400° and 1600° F), it can be concluded that the increased precipitate volume at 1400° F is made up of atoms not contributing to the relatively large value of the random atomic displacement in unaged material.

In summing up these preliminary results of the intensity measurements, it appears that the average random atomic displacement of the matrix atoms is a fundamental property of a solid solution. Such a solid solution could be a stable one; it could also be an unstable one resulting from the solution treatment of a precipitating system. For those alloys which depend primarily for their high-temperature creep resistance upon solid solution of certain large or incongruous atoms at some temperature (e.g., low-carbon N-155 at 1200° F (reference 1)), this random displacement factor is all important. This is in contrast with alloys which depend upon stress fields surrounding precipitant particles at some particular period in their growth (e.g., Inconel X). For this latter type of structure, the line width measuring techniques give a much better fundamental measurement. These techniques are essentially for measuring larger period strains (or stresses) than the random atomic displacements represented in equation (1).

## Mechanical Behavior at 1200° F

Rupture-test properties.- Figure 14 shows the influence of aging upon the time for rupture, at 1200° F under a stress of 100,000 psi. The effect bears striking resemblance to the effect of aging upon internal strains (see fig. 11); in fact, the correlation is very satisfactory. However, at lower stresses, considerable reshuffling of the relative rupture strengths occurs, as shown by the 1000-hour rupture strengths which are practically independent of aging conditions.

In figures 15 to 17 the more conventional curves of rupture stress against rupture time are shown with aging times as parameters. Inspection of these figures shows that the materials unaged and aged for time periods sufficient to obtain relatively long rupture times at the higher stresses (of the order of 100,000 psi) and broad diffraction lines (high internal strains) exhibit an s-shaped transition to a lower rupture strength curve, the transition time increasing with increased aging time. On the other hand, materials overaged from the standpoint of internal strains and with intermediate short-time rupture strengths have relatively constant slopes. The net result then is that, when considering stresses for rupture between 100 and 1000 hours, the initially superior aged material has become, for all practical purposes, no better than all the other aged materials.

Examination of the fractures of the various samples at both short (approximately 1 hr) and longer (approximately 100 hr) rupture times (see fig. 18) reveals that at the short rupture times the fractures are in general a combination of transgranular and intergranular fractures; at the longer rupture times, the fractures are predominately intergranular. Table V(a) shows that coincident with this shift in the mode of fracture there was a lowering of the true strain at the fracture for all samples.

In addition, at the short rupture times, shear-type failures, failures along planes at approximately 45° to the direction of stressing, were frequently observed in all the various aged materials while none were observed in samples ruptured at stresses less than 65,000 psi. As might therefore be expected, fracture surfaces at the higher stresses showed evidences of flow, especially on those fractures which are of a shearing type. When the fracture crack propagated through a grain rather than a grain boundary, the crack had a characteristic jagged or rough appearance in contrast with the smooth appearance of the intergranular cracks. Lastly, figures 19 and 20 show that as the fracture stresses are lowered from 65,000 to 50,000 psi creep rates of the various aged materials become extremely small.

Fracture mechanism.- In accordance with the previously discussed experimental facts, two mechanisms of fracture in solution-treated and aged Inconel X alloy are proposed. It is first proposed that at high stresses and short fracture propagation times with corresponding high creep rates, the fracture resistance is controlled by the matrix. Any variation of the matrix resistance to fracture in this high stress range is due to variations in the matrix internal strains as a result of various aging treatments. Whether this is due to variation of internal stress or variation of the number of defects introduced into the matrix from creep occurring before fracture has not been ascertained. Both mechanisms are possibly at work. In any event, the fact that matrix internal strains (i.e., matrix strength) control rupture strength at high stresses explains the results shown in figure 14 and the fact that the fracture surfaces are, at least in part, transgranular at these high stresses. Also, shear fractures are usually associated with large amounts of deformation before fracture (noted from lectures given by Dr. John E. Dorn during 1948 at the Univ. of Mich.).

At the longer rupture periods (greater than 100 hr), it is further proposed that rupture strength is controlled by the character of the grain boundaries. This is consistent with the fact that at the lower rupture stresses (and longer rupture times) all the various aged specimens had intergranular fractures. Since all the various aged materials had rupture strengths in the intergranular region which were approaching a common value, it can be concluded from the above postulate that the prior aging conditions had a smaller influence on the rupture strength of the grain boundary regions than on the rupture strength of the matrix. Such a conclusion can be subject to experimental verification possibly through internal friction measurements of the type recently popularized by Ke (see reference 5).

Another feature of the two postulates is that it is unnecessary to assume some sort of structural instability to explain the changes in slope or direction of the various rupture curves; that is, each of these fracture mechanisms has its own characteristic curve. The entire rupture

curve for a given aged condition will be equal to the lower of the two curves at any time period. Figure 21 shows this effect schematically. It will be noticed that in order to fit the experimental curves obtained, a rather sharp curvature upward of the grain boundary rupture curves is necessary at short time periods. This is at variance with the rate theory at present and suggests that revisions of such theories will have to be made if the postulates contained herein are correct.

Re-examination of figures 15 to 17 with the schematic diagram of figure 21 shows that aging does have some effect on the grain-boundary rupture strengths. This effect is principally shown by the position of the transitions from matrix-controlled to grain-boundary-controlled fracture. In general, it appears that as aging progressed the time at which the transition period appeared reached a maximum and then diminished slightly. Note the movement of the transition period to the right in figure 16 and the maximum in the time at which transition appeared in figure 17. The fact that the time at which the period of transition took place does not appear to correlate with internal matrix strains cannot be explained at present; however, it can be cited as the reason for the reshuffling of rupture strengths at the longer rupture times when compared with short-time strengths.

Creep characteristics.- Immediately evident from figures 19 and 20 is the very marked influence of aging upon the creep rate at 1200° F under stresses of 65,000 and 50,000 psi. Furthermore, the behavior at both stresses appears qualitatively to be the same. Unfortunately, the creep rates in the more creep-resistant materials at 50,000 psi were so low that they were below the sensitivity of the extensometer used. The tests were run until the specimen fractured or for periods comparable with the fracture time.

Another outstanding characteristic of Inconel X is that, despite the relatively low creep rates observed at 65,000 psi in many of the aged conditions, 65,000 psi corresponded roughly to the 100-hour rupture strength of these same materials. As table VI(a) shows, stresses giving comparable creep rates with those of low-carbon N-155 (see reference 1) are roughly equivalent to the 100-hour rupture strength of the material; that is, the 100-hour rupture strengths of the two materials, while not greatly dissimilar, result in greatly dissimilar creep rates (see table VI(b)). Because Inconel X in general has such high resistance to creep associated with its 100- or 1000-hour rupture stresses at 1200° F, the total deformation to fracture is low and the alloy is commonly characterized as being brittle around 1200° F. Examination of the strains at fracture in table V(a) and comparison with the values reported for solution-treated and aged N-155 alloy make this clear. It thus appears that better advantage of the outstanding creep resistance of the alloy could be taken by raising its rupture strength.

Also of importance is the primary creep that is observed in the various aged specimens. For example, primary creep may be of sufficient magnitude to overshadow any so-called "secondary creep" that occurs during the expected life of the component. Examination of figure 22 shows a relationship between primary creep and aging at temperatures of 1400° and 1600° F and stresses of 65,000 and 50,000 psi. No primary creep was observed with the specimens aged 100 or 1000 hours at 1200° F. In all cases, primary creep was measured as the extension from the initial extension to the point at which the creep curve had reached the reasonably steady-state secondary rate. Ten hours was sufficient for this to occur in all specimens tested.

A rough correlation was found that showed that no primary creep occurred when the stress used for the test was 80 percent of the 0.02-percent-offset yield stress or below for the particular aged condition being considered. No further correlation between amount of primary creep and the ratio of creep stress to yield stress was apparent from the data. Comparison of figure 22 with figures 19 and 20 shows primary creep to be of negligible importance except for material aged for 1000 hours at 1400° F. Furthermore, except for this material, the amount of primary creep appeared to be qualitatively following the rate of secondary creep. As to why long aging at 1400° F results in large primary creep with moderate secondary creep, no answer is apparent at present. Various investigators have reported that primary creep is recoverable so perhaps the anelastic characteristics of the alloy should be considered.

Relation between internal structure and creep characteristics.- Comparison of figure 19 with figure 11 shows an apparent connection between the secondary creep rate and the internal strains as measured by diffraction-line widths. Figure 23 shows the correlation. Considering the magnitude of the errors involved in measuring both line widths and creep rates, the correlation can be considered satisfactory. An extension of the reaction rate theory of creep to cover the effects of internal stress shows that logarithmic creep rate can be expected to be a linear function of internal stress (or strain). In accordance with Eyring and others (see for example reference 6), the creep process is assumed to be one of activating small units of flow and their subsequent jumps in either direction relative to the applied shear stress. The creep rate is the difference between the rate of jump in the two directions and the resulting expression becomes

$$\dot{\epsilon} = \text{Constant} \times T \times e^{\frac{\Delta S}{R}} e^{-\frac{\Delta H}{RT}} \sinh\left(\frac{\text{Constant} \times \tau}{RT}\right) \qquad (3)$$

where

H enthalpy of activation process, (cal)/mole

| | |
|---|---|
| $R$ | gas constant, (cal)/$^{o}$K/mole |
| $S$ | entropy of activation process, (cal)/($^{o}$K)(mole) |
| $T$ | temperature, $^{o}$K |
| $\dot{\epsilon}$ | creep rate, (in.)/(in.)/(hr) |
| $\tau$ | shear stress, psi |

When considering materials with internal stresses (or strains), satisfaction of equilibrium conditions results in the stresses appearing in regions of positive and negative sense. Then, in alternating regions, the sense of the internal stress will be opposite to the sense of the applied stress; in the remaining regions, the sense will be the same as the applied shear stress ($\tau$ of equation (3)). However, if the periodicity of these alternating stresses is assumed to meet certain requirements which will be subsequently discussed, the regions of internal stresses opposite to the sense of the applied stress will effectively control the creep rate. For these regions, equation (3) becomes

$$\dot{\epsilon} = \text{Constant} \times T \times \dot{e}^{\frac{\Delta S}{R}} e^{-\frac{H}{RT}} \sinh \left[\frac{\text{Constant} \times \left(\tau - \bar{\sigma}_i\right)}{RT}\right] \qquad (4)$$

where $\bar{\sigma}_i$ is the effective internal stress. For $\left[\text{Constant} \times \left(\tau - \bar{\sigma}_i\right)\right] \ll RT$, equation (4) can be rewritten in the form

$$\log \dot{\epsilon} = \text{Constant} + \log T + \frac{\Delta S}{R} - \frac{H}{RT} + \text{Constant} \times \left(\frac{\tau - \bar{\sigma}_i}{RT}\right) \qquad (5)$$

For a series of tests at constant temperature and constant $\tau$ but with varying $\bar{\sigma}_i$, equation (5) becomes

$$\log \dot{\epsilon} = \text{Constant} - \text{Constant} \times \bar{\sigma}_i \qquad (6)$$

which is the relation appearing graphically in figure 23, provided the assumption is made that $\bar{\sigma}_i$ is a linear function of line width as measured here. An alloy whose creep behavior at a particular temperature satisfies equation (5) or its modification, equation (6), will be defined as a precipitation-strengthened alloy at that temperature. Satisfaction of equation (5) is again dependent upon the strain centers, that is, the precipitate particles, being in a certain "critical dispersion." This critical dispersion will be subsequently discussed.

Considerable criticism has been leveled at the theoretical results obtained when the Eyring reaction rate theory has been applied to the

creep of metals. It has been found that over wide ranges of stress, temperature, or both the results do not agree with the predictions of the theory. This, however, is to be expected since the so-called "constants" of the theoretical creep rate expression are probably functions of the above-named variables. However, there is at present no reason to suspect that over a small temperature and/or stress variation the theory is not correct. It is felt that in the case covered herein, the effective stress variation is small enough to expect that the reaction rate theory of creep would apply. It must be admitted, however, that the assumption of a linear relationship between $\bar{\sigma}_1$ and line width, as measured herein, was the simplest that could be made. This assumption is apparently correct.

Yield strengths.- Of practical importance and some theoretical value is the yield point of a metal. For these reasons, yield-point determinations were made at 1200° F on the various aged materials. Figure 24 shows the results obtained. Qualitatively, the curves resemble the curves of figures 10 and 11 relating hardness and internal strain to aging, respectively. The correlation of yield point at 1200° F with hardness at room temperature is shown in figure 25 and is as satisfactory as widely used correlations of yield point with hardness for low-alloy structural steels.

A correlation of the 1200° F yield point with internal strain was also attempted to verify or reject the Taylor hypothesis regarding yield (see reference 7). Taylor's hypothesis essentially states that a metal yields when the external stress is such as to make all the internal stresses of the same sign. Assuming a conversion of internal strain to internal stress with appropriate elastic constants, Taylor's theory means that yield stress should be a linear function of internal strain. A plot of yield stress at 1200° F against line width is shown in figure 25. It is obvious that a linear relation is not obtained; hence, the Taylor theory must be imperfect in some respect. The most obvious difficulty is that in the temperature range considered strain rate is probably more closely a function of stress than strain alone. Yield point is a function of rate of loading as a consequence.

## Mechanical Behavior at 1500° F

Figure 26 shows the behavior at 1500° F of Inconel X alloy in the rupture test and figure 27 shows the behavior in the creep test. Only the effects of aging at 1600° F were investigated. It is evident when considering the speed of the precipitation reaction at 1200° and 1400° F that the unaged material is very unstable at 1500° F. For example, the precipitation reaction proceeds to a fair degree of completion during the duration of the standard 1000-hour creep test.

As is evident from figure 26, aging did nothing but uniformly reduce the resistance to rupture. Examination of the fracture surfaces shows both intergranular and transgranular failures (see fig. 28). No transition from mixed to wholly intergranular failures occurred at longer rupture times within the range of this investigation. Also, the amount of creep which took place at stresses equal to the 100- or 1000-hour rupture stresses was considerably larger than that which took place at the corresponding stresses at 1200° F.

These results strongly suggest that the fracture at 1500° F was controlled by the matrix strength and certainly not by the internal strains due to precipitation. These internal strains are of small magnitude and do not correlate with the relative rupture resistance at 1500° F of the various aged conditions (see figs. 11 and 26). However, as noted previously, one effect of aging at 1600° F was to reduce uniformly the random atomic displacements in the matrix by rejection of the precipitant atoms to form the precipitate readily visible after such aging. This then is most probably the way in which matrix control is exerted over the resistance to rupture. It is tacitly assumed that with a given stress, rupture crack propagation is slower the greater the random atomic displacements because of the presence of the precipitant or incongruous atoms in random solution. Under this hypothesis, the unaged material will have superior rupture strength only so long as precipitation has not progressed far enough to deplete the matrix of the precipitant atoms.

Examination of figure 27 shows that aging at 1600° F did nothing but reduce the resistance to creep at 1500° F. The parallelism with the effects of aging on rupture strength is quite striking. Indeed, the same mechanism may be assumed to control in both cases - namely, reduction of the random displacements of the matrix atoms through precipitation.

It must be admitted that figure 27 is only an imperfect representation of the facts. The so-called "secondary creep period" was nearly nonexistent because of the presence of early and prominent tertiary creep. Figure 29 shows three typical time-elongation curves for the tests at 1500° F. It is felt that the tertiary creep can be attributed to changes of internal structure (rather than necking down of the specimen cross-sectional areas). The total creep was increasing at such slow rates at the onset of the tertiary creep stages that sufficient increase of stress to cause the increasing creep rates seemed implausible. On the other hand, increase in time of prior aging at 1600° F would decrease the time necessary at 1500° F to complete effectively the precipitation reaction (depletion of the precipitant atoms in the matrix). Furthermore, the reaction rate at 1500° F under stress is quite probably rapid enough to make the additional time needed of small magnitude. This decrease in necessary aging time at 1500° F with increased aging at 1600° F prior to test should result in the appearance of earlier tertiary creep. This is clearly the case. The tertiary region may be interpreted as the approach to a creep rate representative of the matrix with the random atomic displacements removed as a result of rejection of the precipitant atoms.

## COMPARISON WITH PREVIOUS WORK ON LOW-CARBON N-155

When the results of this investigation are compared with the previous work on low-carbon N-155 (see reference 1), a distinct difference in behavior is evident. On one hand, solution-treated and aged Inconel X at 1200° F obeys the previously discussed extension of the reaction rate theory which states that logarithmic creep rate at fixed stress (and temperature) is proportional to the internal strains resulting from precipitation - the greater the internal strain, the smaller the rate. On the other hand, solution-treated and aged low-carbon N-155 at 1200° F was found to have creep rates, at a given stress, which did not decrease with increasing internal strain from precipitation but increased. The hypothesis offered in the earlier work was that the spacing between the strain centers in low-carbon N-155 (precipitate particles) was too large to interrupt effectively the slip system operating during creep. The spacing of precipitate particles at the maximum internal strain observed was of the order of $10^{-4}$ centimeter in this alloy.

Immediately evident is the fact that high internal strains in Inconel X occur at much smaller precipitate spacings than $10^{-4}$ centimeter. At 1400° F, maximum strains occur with the average spacing between precipitant particles or strain centers not larger than $5 \times 10^{-5}$ centimeter (see electron micrograph of sample aged 30 hr at 1400° F, as shown in fig. 8(b)). Higher internal strains occurred after extended aging at 1200° F. Unfortunately, the electron micrographs revealed very little in this case because the particles of precipitate at this stage are probably below the limit of resolution of the microscope. The spacing is certainly smaller at 1200° F than at 1400° F which means that the spacing is less than $5 \times 10^{-5}$ centimeter. A fair estimate of the spacing is probably $5 \times 10^{-6}$ centimeter. The difference then in the interrelation of the internal strains of precipitation and creep at 1200° F between N-155 and Inconel X is a matter of precipitate particle (strain center) spacing; the spacing in the latter alloy is small enough to interrupt effectively a major portion of the slip systems operating during creep while the spacing in the former alloy is not.

A quantitative analysis of this problem has recently been published (reference 8) in which it is ascertained that a critical dispersion of the precipitate particles exists. If the spacing of the precipitate is too large, dislocations can move relatively freely through the areas free of precipitate. If the spacing is too small, the strains surrounding the particles overlap to a certain extent on a dislocation and their effect is lost. With the critical spacing, dislocations are bent into a wavy form in their movement forward, by being in part forced through the interstices between precipitate particles and in part curled around the particles. The process can be visualized as being somewhat like forcing a rubber string transversely and horizontally through a system of vertical

rods. This critical spacing was found to be related to certain other properties through the relation:

$$\Lambda = \frac{Ga}{\sigma_y} \tag{7}$$

where

| | |
|---|---|
| a | interatomic spacing, A |
| G | shear modulus, psi |
| $\Lambda$ | critical spacing of precipitate, centimeters |
| $\sigma_y$ | yield stress, psi |

Making the assumptions that $G = 10^7$ psi, that $\sigma_y \approx 5 \times 10^4$ psi, and that $a = 3.5$ A for either Inconel X or low-carbon N-155 (the differences in these quantities for these two alloys is of small magnitude), $\Lambda$ is found to be of the order of 700 A or $7 \times 10^{-6}$ centimeter. The previously stated precipitate spacings for Inconel X and low-carbon N-155 alloys clearly show that the latter exceeds the critical value by one to two orders of magnitude while the former is approximately the same order of magnitude as the critical value. Thus, Inconel X obeys the previously discussed extension of the reaction rate theory of creep while low-carbon N-155 does not. With low-carbon N-155 alloy, the effect of aging is to remove short-period strains surrounding the precipitant atoms in random solid solution. While, in keeping with the above analysis, the original precipitate dispersion may be below the critical value for the alloy, replacing it with another that far exceeds the critical value can easily result in a net reduction in the resistance to creep. Behavior of Inconel X aged at 1600° F prior to test at 1500° F was also clearly of this type.

## CONCLUSIONS

Studies were made of the mechanisms by which various aging treatments influenced the mechanical properties of solution-treated Inconel X alloy for time periods up to 1000 hours at test temperatures of 1200° and 1500° F. Microstructural analyses at the various aged conditions were made by means of X-ray diffraction studies and optical- and electron-micrographic examinations.

From correlations of the mechanical properties with the structural analyses and from comparisons with the previously determined aging effects on low-carbon N-155 alloy, two classes of austenitic alloys are established and the following conclusions are drawn:

1. The Mott and Nabarro criterion of precipitate dispersion for effective impedance of dislocations explains satisfactorily the fact that the creep resistance of Inconel X can be improved by precipitation and that the creep resistance of low-carbon N-155 is not. The critical precipitate dispersion is exceeded by one or more orders of magnitude in the latter alloy and is closely equaled in the former.

2. Extension of the reaction rate theory shows that, for the critical precipitate dispersions, the logarithmic creep rate is a linear function (with negative slope) of the internal stresses surrounding the precipitate particles. This was verified experimentally with Inconel X at 1200° F.

3. At 1500° F, where internal strains due to precipitation are small and the precipitate dispersions are too large, Inconel X exhibits loss of creep resistance when aged. This loss is due to reduction of random atomic displacements in the matrix by rejection of the precipitate atoms. Low-carbon N-155 at 1200° F also exhibits the same behavior.

4. Rupture strength of Inconel X in the stress region of high creep rates at 1200° F and 1500° F is apparently under control of the matrix and fractures are both transgranular and intergranular. More specifically, internal strains due to precipitation and random atomic displacements due to presence of precipitate atoms in random solid solution control at 1200° and 1500° F, respectively.

5. In the region of low creep rates at 1200° F, rupture of Inconel X becomes intergranular and dependent upon the character of the grain boundaries. A characteristic change in curvature connects the rupture curve in the region of matrix control to the region of grain boundary control.

University of Michigan
Ann Arbor, Mich., August 18, 1949

# APPENDIX

## PROCESSING SCHEDULE FOR INCONEL X 1-INCH ROUND BAR STOCK FROM MELT Y3724-X

The processing of the Inconel X bar stock was reported to be as follows:

(1) Charge of 9400 pounds melted in induction furnace and cast into two 18-inch by 18-inch by 4400-pound ingots; transferred hot to hammer shop

(2) Ingots heated to 2225° F and forged to 14-inch blooms; reheated and forged to 12-inch blooms; reheated, forged to 12-inch rounds, and air-cooled

(3) Surfaces overhauled by machining to remove external defects

(4) Machined rounds forged to 8-inch blooms, cut in half, and air-cooled

(5) Blooms heated to 2225° F, rolled to 3-inch by 3-inch by 160-pound billets, and air-cooled

(6) Billets heated to 2200° F, cogged to 2-inch-square billets, and quenched; sheared into three equal lengths and ground all over

(7) Heated to 2200° F, rolled to $1\frac{3}{32}$-inch rounds, and quenched; approximate finishing temperature, 1800° to 1900° F

(8) Rounds straightened on Medart straightening rolls

(9) Test specimens cut from each end of each round and macroetched

(10) Brightman turned to 1-inch diameter

(11) Rods inspected for surface seams and then given one pass through production grinder

## REFERENCES

1. Frey, D. N., Freeman, J. W., and White, A. E.: Fundamental Effects of Aging on Creep Properties of Solution-Treated Low-Carbon N-155 Alloy. NACA Rep. 1001, 1950.

2. Mott, N. F., and Nabarro, F. R. N.: Estimation of Degree of Precipitation Hardening. Proc. Phys. Soc. (London), vol. 52, pt. 1, Jan. 1940, pp. 86-89.

3. Darwin, C. G.: Reflection of X-Rays from Imperfect Crystals. Phil. Mag., vol. 43, May 1922, pp. 800-829.

4. Hengstenberg, J., and Mark, H.: Röntgenographische Intensitätsmessungen an Gestörten Gittern. Zeitschr. Phys., Bd. 61, Heft 7-8, 1930, pp. 435-453. Röntgenographische Untersuchung von Gitterstörungen in Leichtmetallen. Zeitschr. Elektrochem. und angewandte phys. Chem., Bd. 37, Heft 3, 1931, pp. 524-528.

5. Kê, T'ing-Sui: On the Structure of Grain Boundaries in Metals. Phys. Rev., vol. 73, no. 3, Feb. 1, 1948, pp. 267-268.

6. Dushman, Saul, Dunbar, L. W., and Huthsteiner, H.: Creep of Metals. Jour. Appl. Phys., vol. 15, no. 2, Feb. 1944, pp. 108-124.

7. Taylor, G. I.: Plastic Deformation of Crystals. Proc. Roy. Soc. (London), vol. 145, July 2, 1934, pp. 362-404.

8. Mott, N. F., and Nabarro, F. R. N.: Dislocation Theory and Transient Creep. Conf. on Strength of Solids, Phys. Soc. (London), 1948.

TABLE I

MECHANICAL TESTING SCHEDULE

| Prior treatment | Test temperature (°F) | Test stress (psi) | Type of test |
|---|---|---|---|
| Unaged | 1200 | ------ | Rupture times from 1 to 1000 hr |
| | 1500 | ------ | Rupture times from 1 to 1000 hr |
| | 1200 | 65,000 | Creep and yield-point determination |
| | 1200 | 50,000 | Creep test |
| | 1500 | 25,000 | Creep test |
| | 1500 | 15,000 | Creep test |
| Aged 100 hr at 1200° F | 1200 | ------ | Rupture times from 1 to 1000 hr |
| | 1200 | 65,000 | Creep test |
| | 1200 | ------ | Yield-point determination |
| Aged 1000 hr at 1200° F | 1200 | ------ | Rupture times from 1 to 1000 hr |
| | 1200 | 65,000 | Creep test |
| | 1200 | ------ | Yield-point determination |
| Aged 1 hr at 1400° F | 1200 | ------ | Rupture times from 1 to 1000 hr |
| | 1200 | 65,000 | Creep test |
| | 1200 | 50,000 | Creep test |
| | 1200 | ------ | Yield-point determination |
| Aged 10 hr at 1400° F | 1200 | ------ | Rupture times from 1 to 1000 hr |
| | 1200 | 65,000 | Creep test |
| | 1200 | 50,000 | Creep test |
| | 1200 | ------ | Yield-point determination |
| Aged 100 hr at 1400° F | 1200 | ------ | Rupture times from 1 to 1000 hr |
| | 1200 | 65,000 | Creep test |
| | 1200 | 50,000 | Creep test |
| | 1200 | ------ | Yield-point determination |
| Aged 1000 hr at 1400° F | 1200 | ------ | Rupture times from 1 to 1000 hr |
| | 1200 | 65,000 | Creep test and yield-point determination |
| | 1200 | 50,000 | Creep test |
| Aged 1 hr at 1600° F | 1200 | ------ | Rupture times from 1 to 1000 hr |
| | 1500 | ------ | Rupture times from 1 to 1000 hr |
| | 1200 | 65,000 | Creep test and yield-point determination |
| | 1200 | 50,000 | Creep test |
| | 1500 | 25,000 | Creep test |
| | 1500 | 15,000 | Creep test |
| Aged 10 hr at 1600° F | 1200 | ------ | Rupture times from 1 to 1000 hr |
| | 1500 | ------ | Rupture times from 1 to 1000 hr |
| | 1200 | 65,000 | Creep test and yield-point determination |
| | 1200 | 50,000 | Creep test |
| | 1500 | 25,000 | Creep test |
| | 1500 | 15,000 | Creep test |
| Aged 100 hr at 1600° F | 1200 | ------ | Rupture times from 1 to 1000 hr |
| | 1500 | ------ | Rupture times from 1 to 1000 hr |
| | 1200 | 65,000 | Creep test and yield-point determination |
| | 1200 | 50,000 | Creep test |
| | 1500 | 25,000 | Creep test |
| | 1500 | 15,000 | Creep test |
| Aged 1000 hr at 1600° F | 1200 | ------ | Rupture times from 1 to 1000 hr |
| | 1500 | ------ | Rupture times from 1 to 1000 hr |
| | 1200 | 65,000 | Creep test and yield-point determination |
| | 1200 | 50,000 | Creep test |
| | 1500 | 25,000 | Creep test |
| | 1500 | 15,000 | Creep test |

TABLE II

COMPARISON OF OBSERVED AND THEORETICAL X-RAY LINE INTENSITIES FOR NICKEL POWDER

[Copper $K\alpha_1\alpha_2$ radiation]

| Nickel line | Theoretical $\frac{P_{[HKL]}}{P_{[111]}}$ (1) | Observed $\frac{P_{[HKL]}}{P_{[111]}}$ (1) |
|---|---|---|
| [111] | 1.000 | 1.000 |
| [200] | .48 | .54 |
| [220] | .28 | .25 |

[1] $P_{[HKL]}$ integrated intensity of indicated line.

$P_{[111]}$ integrated intensity of nickel [111] line.

TABLE III

COMPARISON OF OBSERVED AND THEORETICAL X-RAY LINE INTENSITIES FOR INCONEL X

[Copper $K\alpha_1\alpha_2$ radiation]

| Inconel X line | Theoretical $\frac{P_{[HKL]}}{P_{[111]}}$ (1) (2) | Observed $\frac{P_{[HKL]}}{P_{[111]}}$ (1) | | | |
|---|---|---|---|---|---|
| | | Unaged | Aged 1000 hr at 1200° F | Aged 1000 hr at 1400° F | Aged 1000 hr at 1600° F |
| [111] | 0.54 | 0.52 ± 0.05 | 0.44 ± 0.02 | 0.45 ± 0.02 | 0.39 ± 0.02 |
| [200] | .31 | .21 ± 0.02 | .19 ± 0.02 | .26 ± 0.02 | .26 ± 0.02 |
| [220] | .16 | .13 ± 0.02 | .13 ± 0.01 | .16 ± 0.02 | .16 ± 0.02 |

[1] $P_{[HKL]}$ integrated intensity of indicated line.

$P_{[111]}$ integrated intensity of nickel [111] line.

[2] Without extinction or random atomic displacement in Inconel X.

TABLE IV

SUMMARY OF CALCULATIONS FOR X-RAY LINE INTENSITIES OF INCONEL X ALLOY

| Treatment | Mosaic size, d (cm) | Random atomic displacement, $\bar{u}$ (A) |
|---|---|---|
| Unaged | [a]Probably $<10^{-5}$ | Approx. $\pm 0.07$ |
| Aged 1000 hr at 1200° F | Approx. $10^{-5}$ | Approx. $\pm 0.07$ |
| Aged 1000 hr at 1400° F | Approx. $10^{-5}$ | Approx. 0 |
| Aged 1000 hr at 1600° F | Approx. $5 \times 10^{-4}$ | [a]Approx. 0 |

[a]Based on the fact that the observed intensity ratios were, within experimental error, equal to the theoretical values.

TABLE V

RUPTURE-TEST RESULTS FOR SOLUTION-TREATED AND AGED INCONEL X

(a) At 1200° F.

| Prior treatment | Stress (psi) | Rupture time (hr) | True strain at fracture (a) | Elongation in 1 in. (percent) | Reduction of area (percent) |
|---|---|---|---|---|---|
| Unaged | [b]90,000 | ------- | ---- | ---- | ----- |
| | [c]85,000 | ------- | ---- | ---- | ----- |
| | 75,000 | 1.70 | 0.23 | 15 | 19.9 |
| | 70,000 | 1.85 | .17 | 17 | 15.3 |
| | 65,000 | 1.7 | .25 | ---- | 22.5 |
| | 60,000 | 9.70 | .17 | 14 | 16.1 |
| | 60,000 | 4.75 | .16 | 10 | 14.7 |
| | 58,000 | 112 | .12 | 2 | 11.6 |
| | 52,000 | (d) | ---- | ---- | ----- |
| | 50,000 | 400 | .03 | ---- | 2.81 |
| Aged 100 hr at 1200° F | [e]130,000 | ------- | ---- | ---- | ----- |
| | 110,000 | 1.083 | 0.10 | 4 | 9.4 |
| | 90,000 | 2.42 | .17 | 7 | 16.1 |
| | 75,000 | 16.5 | .08 | ---- | 7.8 |
| | 65,000 | 51 | .04 | ---- | 4.06 |
| | 65,000 | 24.5 | .07 | ---- | 6.31 |
| | 55,000 | 559 | .06 | ---- | 4.8 |
| Aged 1000 hr at 1200° F | 130,000 | 0.95 | 0.15 | 13 | 13.8 |
| | 110,000 | 4.00 | .11 | 5 | 10.2 |
| | 90,000 | 26.10 | .10 | 5 | 9.4 |
| | 75,000 | 121 | .03 | 3 | 2.44 |
| Aged 1 hr at 1400° F | 110,000 | 0.067 | 0.21 | 12 | 18.7 |
| | 90,000 | 1.00 | .09 | 3 | 8.5 |
| | 82,000 | 4.75 | .08 | 4 | 7.1 |
| | 65,000 | 39.8 | .10 | 2 | 9.4 |
| | 50,000 | 280 | .02 | ---- | 1.6 |
| Aged 10 hr at 1400° F | 110,000 | 1.00 | 0.12 | 9 | 11.6 |
| | 95,000 | 4.78 | .03 | 3.5 | 3.3 |
| | 80,000 | 31 | .04 | 3 | 4.1 |
| | 70,000 | 42 | .07 | 3 | 6.3 |
| | 60,000 | 108 | .03 | ---- | 2.4 |
| | 51,200 | 172 | .03 | ---- | 3.3 |
| | 50,000 | 362 | >.01 | ---- | >1.0 |
| Aged 100 hr at 1400° F | 110,000 | 0.53 | 0.32 | 21 | 27.5 |
| | 90,000 | 13.4 | .12 | 8 | 11.6 |
| | 80,000 | 45.8 | .02 | 3 | 1.63 |
| | 75,000 | 96.5 | .06 | 3 | 5.50 |
| | 65,000 | 194 | .02 | ---- | 1.63 |
| Aged 1000 hr at 1400° F | [f]130,000 | ------- | ---- | ---- | ----- |
| | 110,000 | 0.33 | 0.42 | 32 | 34 |
| | 95,000 | 1.75 | .32 | 27 | 27.5 |
| | 80,000 | 25.5 | .20 | 15 | 17.5 |
| | 70,000 | 130 | .09 | 2 | 8.5 |
| Aged 1 hr at 1600° F | 95,000 | 0.60 | 0.31 | 23 | 26.7 |
| | 82,000 | 9.17 | .17 | 9 | 15.3 |
| | 82,000 | 3.00 | .20 | 19 | 17.5 |
| | 73,000 | 18.5 | .10 | 9 | 9.4 |
| | 60,000 | 369 | .03 | ---- | 2.44 |
| Aged 10 hr at 1600° F | 95,000 | 1.00 | 0.31 | 27 | 26.7 |
| | 85,000 | (g) | ---- | ---- | ----- |
| | 80,000 | 29.3 | .17 | 11 | 15.3 |
| | 75,000 | 28.5 | .10 | 7 | 9.4 |
| | 65,000 | 379 | .08 | ---- | 7.8 |
| Aged 100 hr at 1600° F | [h]105,000 | ------- | ---- | ---- | ----- |
| | 90,000 | 1.13 | 0.35 | 33.5 | 30.1 |
| | 80,000 | 8.0 | .20 | 10 | 18.3 |
| | 70,000 | 16 | .16 | 16 | 14.7 |
| | 55,000 | 1775 | .04 | ---- | 4.06 |
| Aged 1000 hr at 1600° F | [i]110,000 | -------- | ---- | ---- | ----- |
| | 95,000 | 0.18 | 0.39 | 35 | 32.2 |
| | 80,000 | 3.17 | .51 | 38 | 39.7 |
| | 75,000 | 13.8 | .17 | 13 | 16.1 |
| | 65,000 | 53.5 | .08 | 9 | 7.1 |

[a] $\text{Log}_e \frac{A_o}{A}$
where
$A_o$ original cross-sectional area.
A final cross-sectional area.

[b] Broke at 89,000 psi.

[c] Broke at 83,000 psi.

[d] Discontinued after 268 hr.

[e] Broke at 130,000 psi.

[f] Broke at 128,000 psi.

[g] Discontinued after 1.67 hr.

[h] Broke at 102,000 psi.

[i] Broke at 98,000 psi.

TABLE V

RUPTURE-TEST RESULTS FOR SOLUTION-TREATED AND AGED INCONEL X - Concluded

(b) At 1500° F.

| Prior treatment | Stress (psi) | Rupture time (hr) | True strain at fracture (a) | Elongation in 1 in. (percent) | Reduction of area (percent) |
|---|---|---|---|---|---|
| Unaged | 55,000 | 0.61 | 0.07 | -- | 6.31 |
| | 40,000 | 6.58 | .16 | 7 | 14.7 |
| | 30,000 | 52 | .20 | -- | 18.3 |
| Aged 1 hr at 1600° F | 50,000 | 0.75 | 0.21 | 11 | 18.7 |
| | 40,000 | 3 | .20 | 5 | 17.5 |
| | 30,000 | 20.5 | .16 | 8 | 14.7 |
| Aged 10 hr at 1600° F | 50,000 | 0.41 | 0.38 | -- | 31.7 |
| | 35,000 | 7 | .43 | 28 | 33.6 |
| | 32,500 | 20.5 | .30 | 13 | 26.7 |
| | 25,000 | 88.8 | .15 | 7 | 13.8 |
| Aged 100 hr at 1600° F | 50,000 | 0.51 | 0.21 | -- | 18.7 |
| | 40,000 | 4.08 | .24 | -- | 21.2 |
| | 20,000 | 156 | .24 | 18 | 21.2 |
| Aged 1000 hr at 1600° F | 50,000 | 0.366 | 0.10 | -- | 9.40 |
| | 40,000 | 1.75 | .06 | -- | ----- |

[a] $\log_e \frac{A_o}{A}$

where

$A_o$ original cross-sectional area

$A$ final cross-sectional area

TABLE VI

COMPARATIVE RUPTURE TIMES, STRESSES, AND CREEP RATES AT 1200° F OF LOW-CARBON N-155 AND INCONEL X SOLUTION-TREATED AND AGED 10 HOURS AT 1400° F[a]

(a) Comparable creep rates.

| Alloy | Stress (psi) | Creep rate (in./in./hr) | Rupture time (hr) |
|---|---|---|---|
| Inconel X | 65,000 | $3 \times 10^{-6}$ | 100 |
| Low-carbon N-155 | [b]30,000 | $3 \times 10^{-6}$ | [b]10,000 |

(b) Comparable rupture times.

| Alloy | Stress (psi) | Creep rate (in./in./hr) | Rupture time (hr) |
|---|---|---|---|
| Inconel X | 65,000 | $3 \times 10^{-6}$ | 100 |
| Low-carbon N-155 | 40,000 | [c]$30 \times 10^{-6}$ | 100 |

[a]Treatment selected for combination of creep resistance, rupture strength, and commercial feasibility.

[b]Extrapolated.

[c]Interpolated.

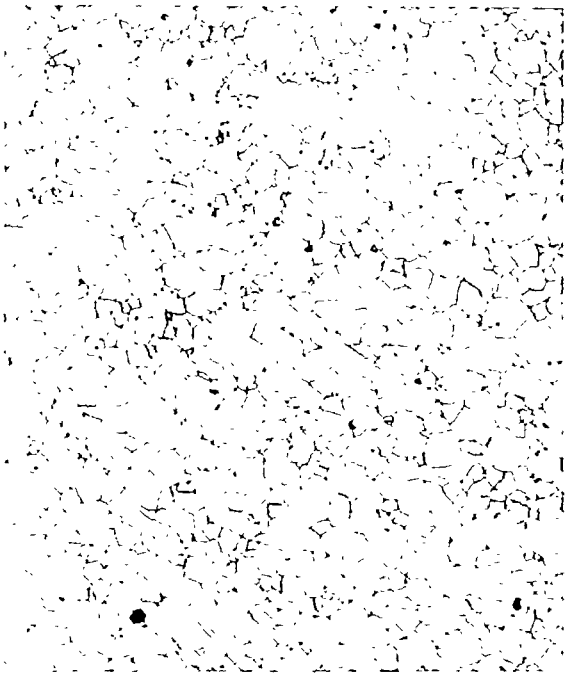

Figure 1.- Microstructure of transverse section of Inconel X bar stock as-rolled. Electrolytically etched in 10 percent oxalic acid. X100.

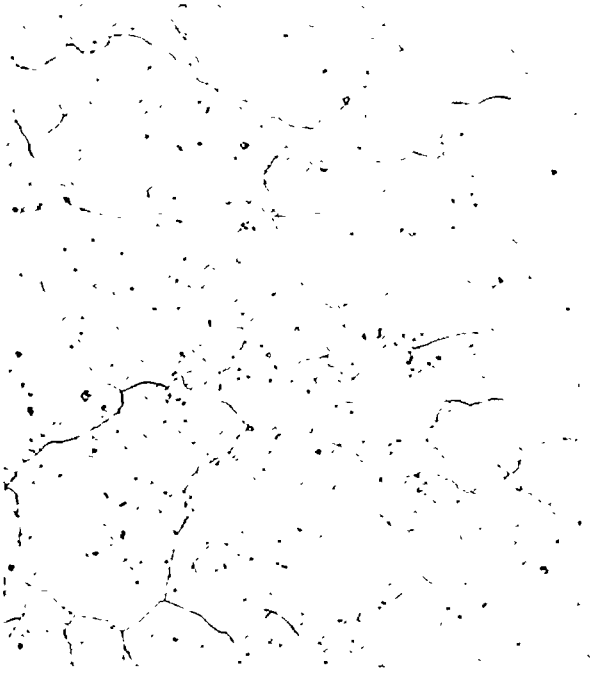

Figure 2.- Microstructure of transverse section of Inconel X bar stock solution-treated 4 hours at 2050° F and water-quenched. Electrolytically etched in 10 percent oxalic acid. X100.

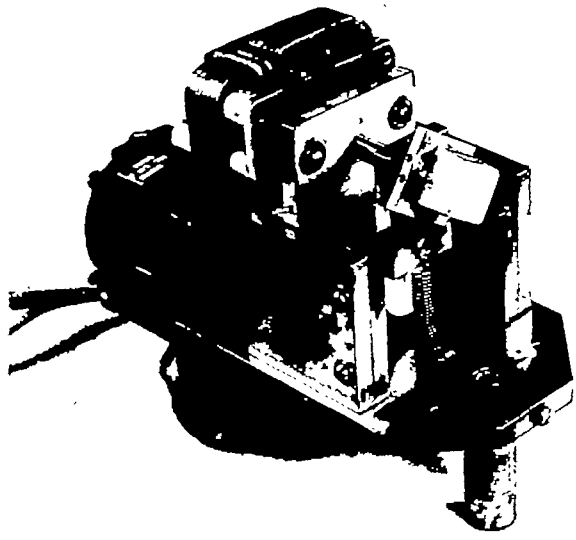

Figure 3.- Specimen mount for Norelco spectrometer.

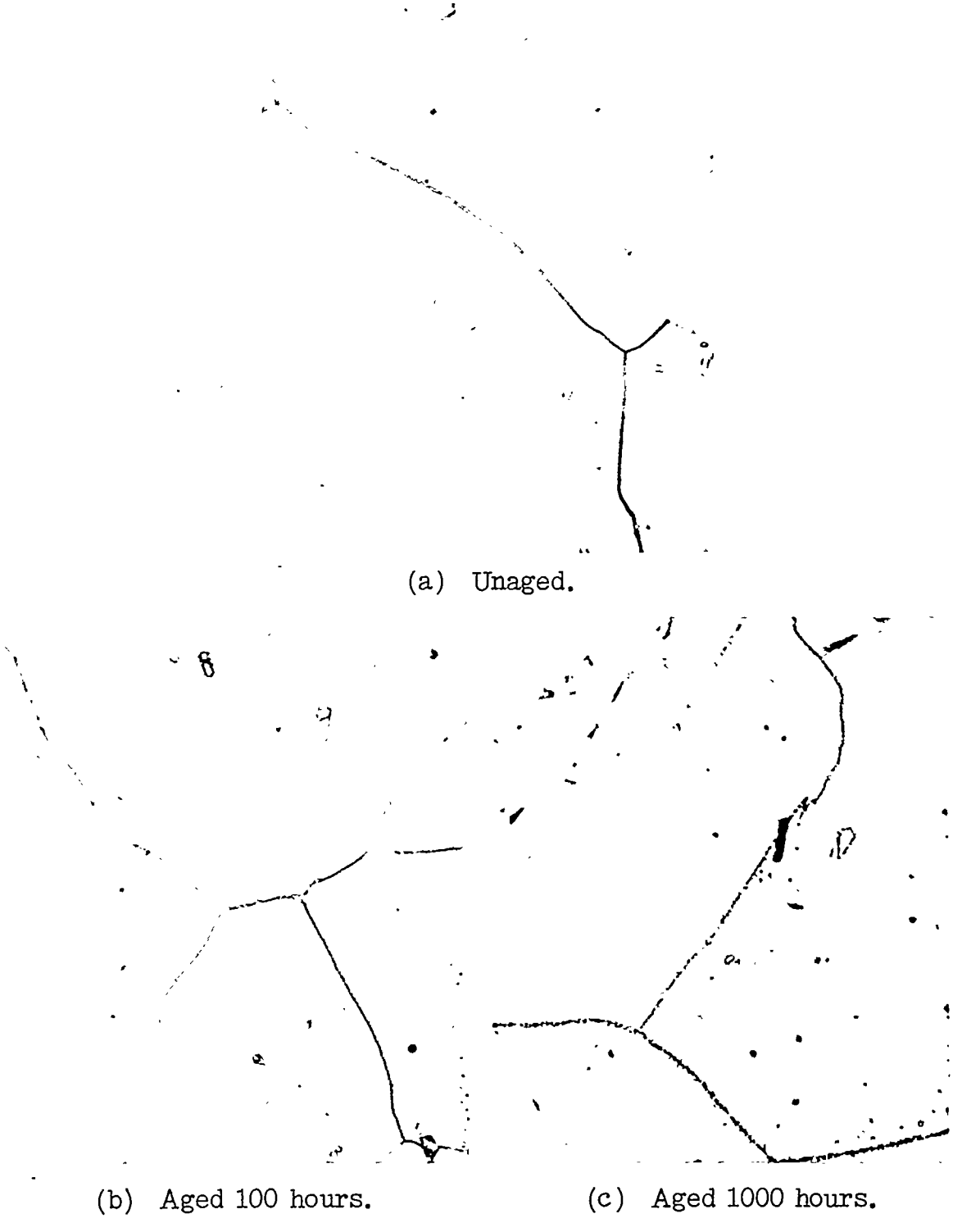

(a) Unaged.

(b) Aged 100 hours.

(c) Aged 1000 hours.

Figure 4.- Effect of aging at 1200° F on microstructure of solution-treated Inconel X alloy. Electrolytically etched in 10 percent oxalic acid. X1000.

(a) Aged 1.0 hour.

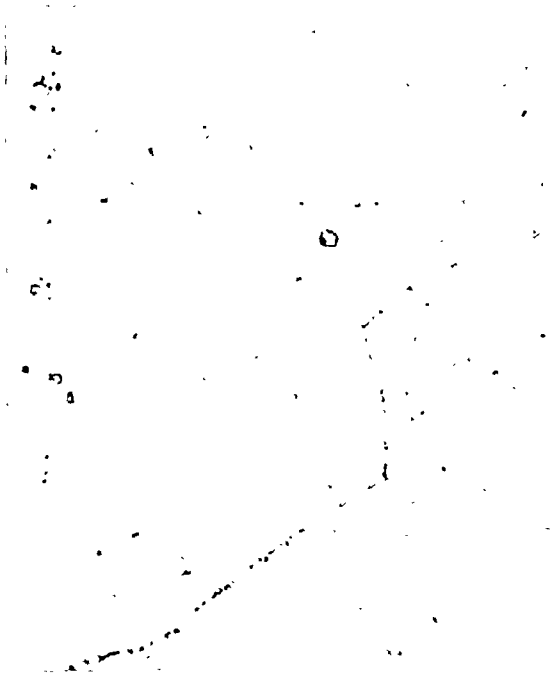

(b) Aged 100 hours.

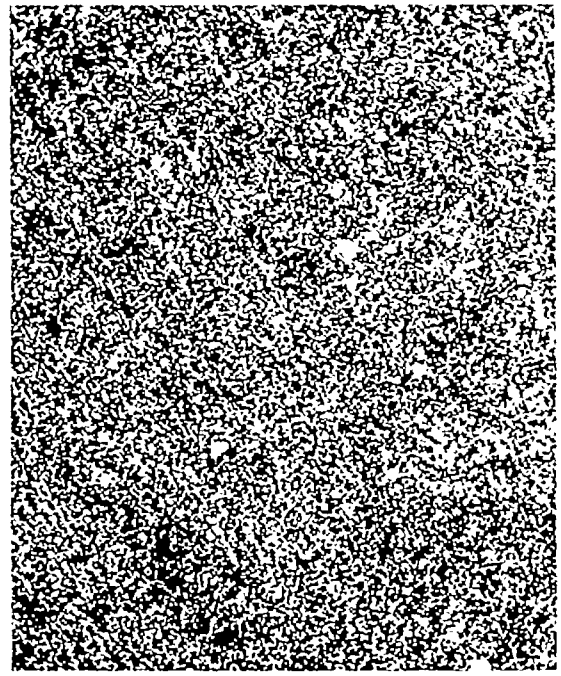

(c) Aged 1000 hours.

Figure 5.- Effect of aging at 1400° F on microstructure of solution-treated Inconel X alloy. Electrolytically etched in 10 percent oxalic acid. X1000.

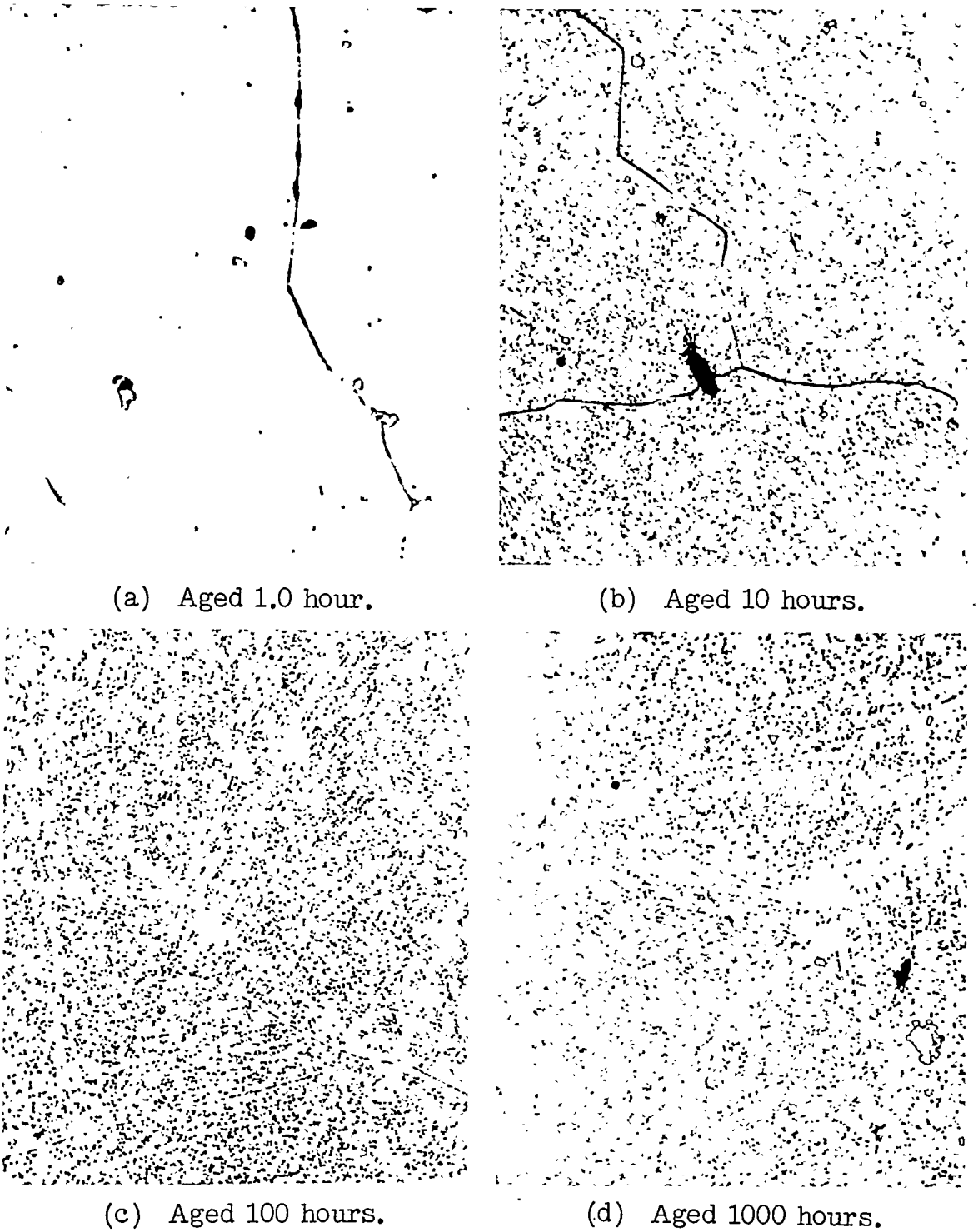

(a) Aged 1.0 hour.

(b) Aged 10 hours.

(c) Aged 100 hours.

(d) Aged 1000 hours.

Figure 6.- Effect of aging at 1600° F on microstructure of solution-treated Inconel X alloy. Electrolytically etched in 10 percent oxalic acid. X1000.

(a) Unaged.

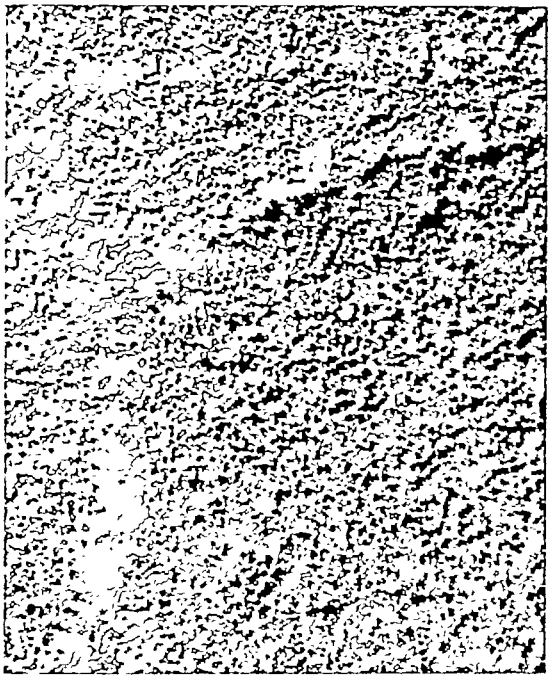

(b) Aged 1000 hours at 1200° F.

Figure 7.- Electron micrographs showing typical microstructures of solution-treated Inconel X alloy. X10,000.

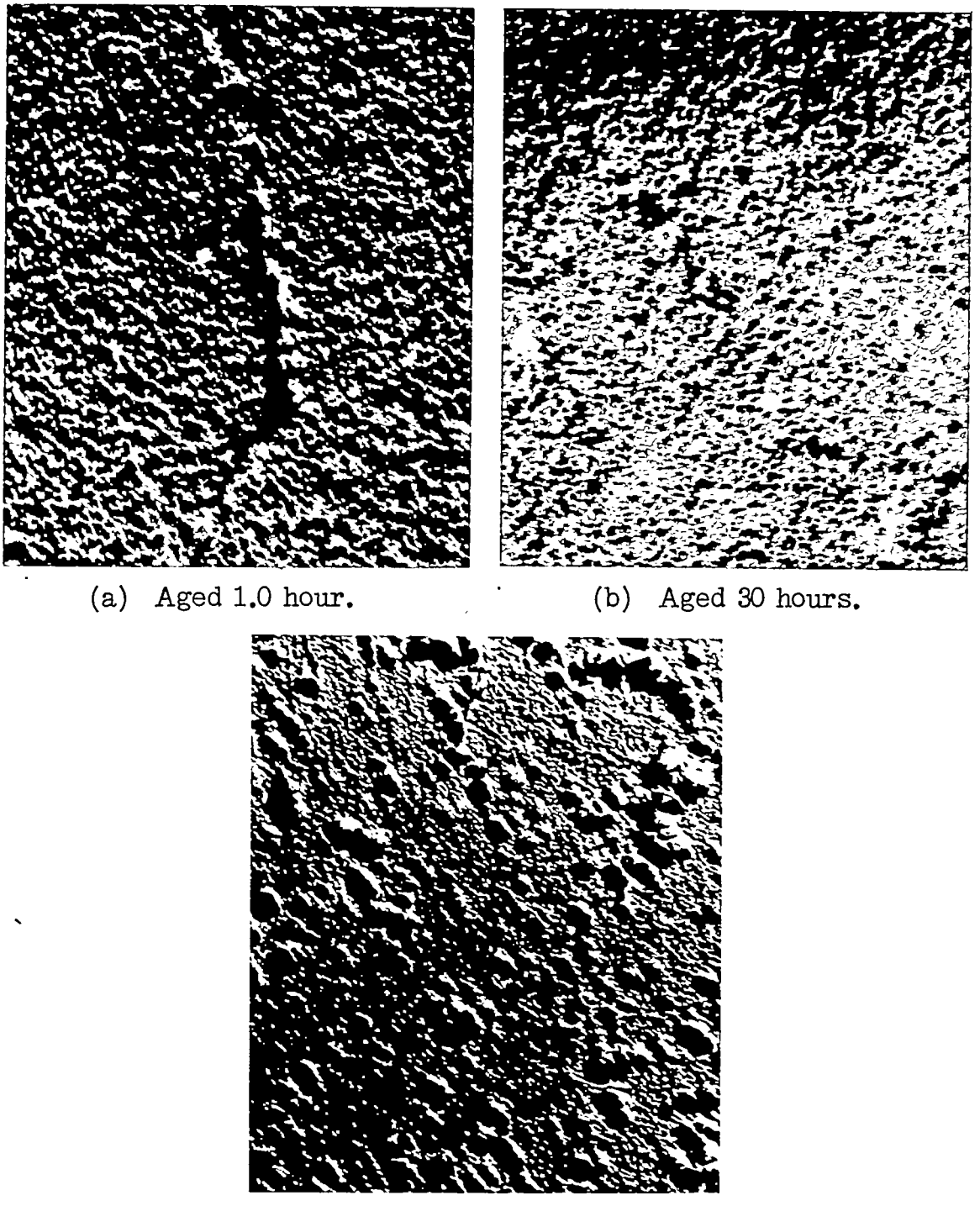

(a) Aged 1.0 hour. (b) Aged 30 hours.

(c) Aged 1000 hours.

Figure 8.- Electron micrographs showing effect of aging at 1400° F on microstructure of solution-treated Inconel X alloy. X10,000.

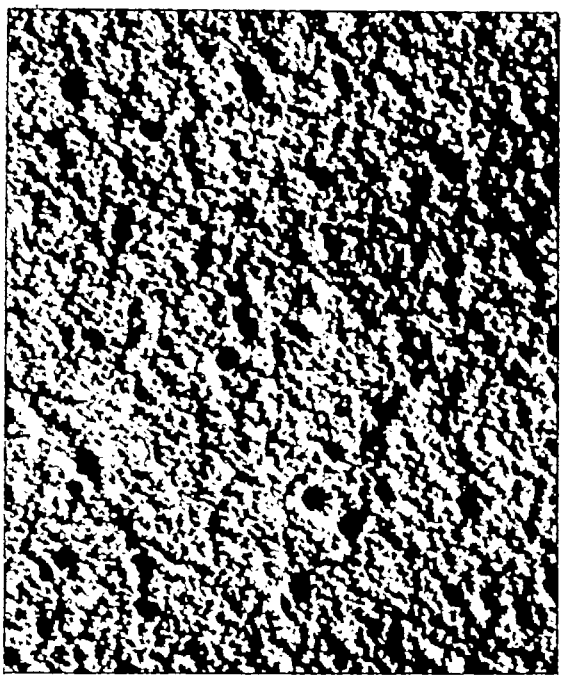

(a) Aged 10 hours.

(b) Aged 1000 hours.

Figure 9.- Electron micrographs showing effect of aging at 1600° F on microstructure of solution-treated Inconel X alloy. X10,000.

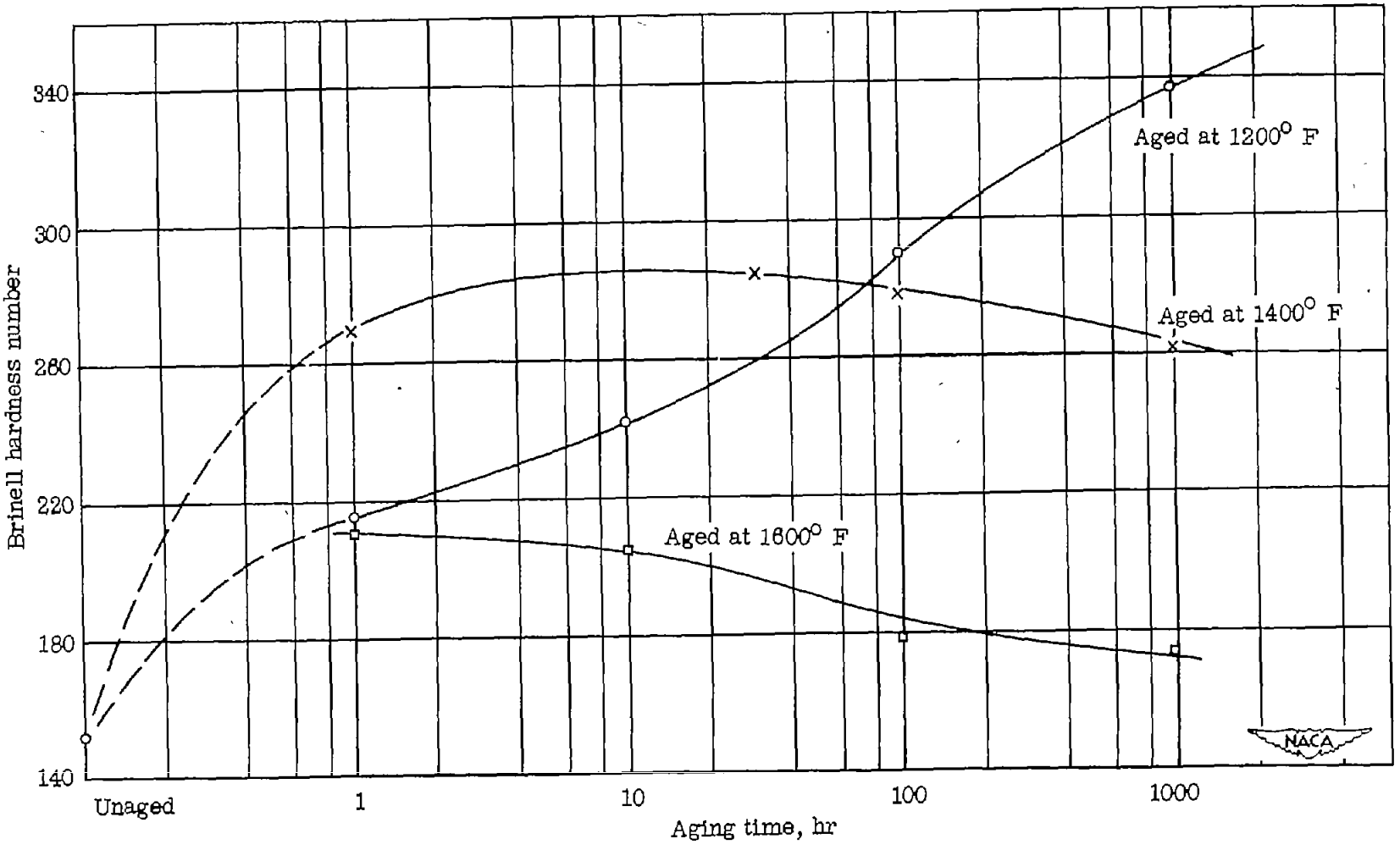


Figure 10.- Effect of aging on hardness of solution-treated Inconel X alloy.

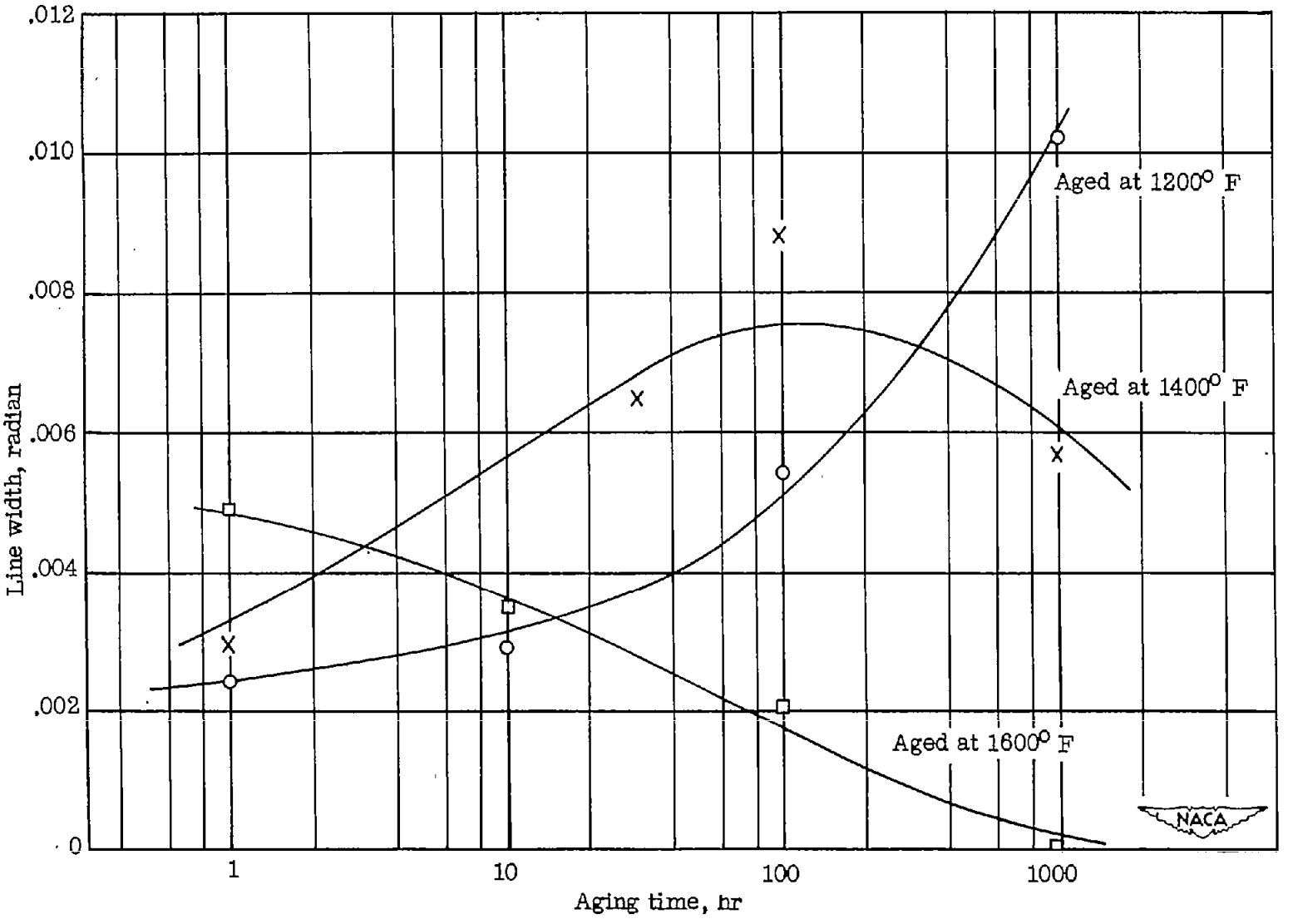


Figure 11.- Effect of aging on internal strain of solution-treated Inconel X alloy.

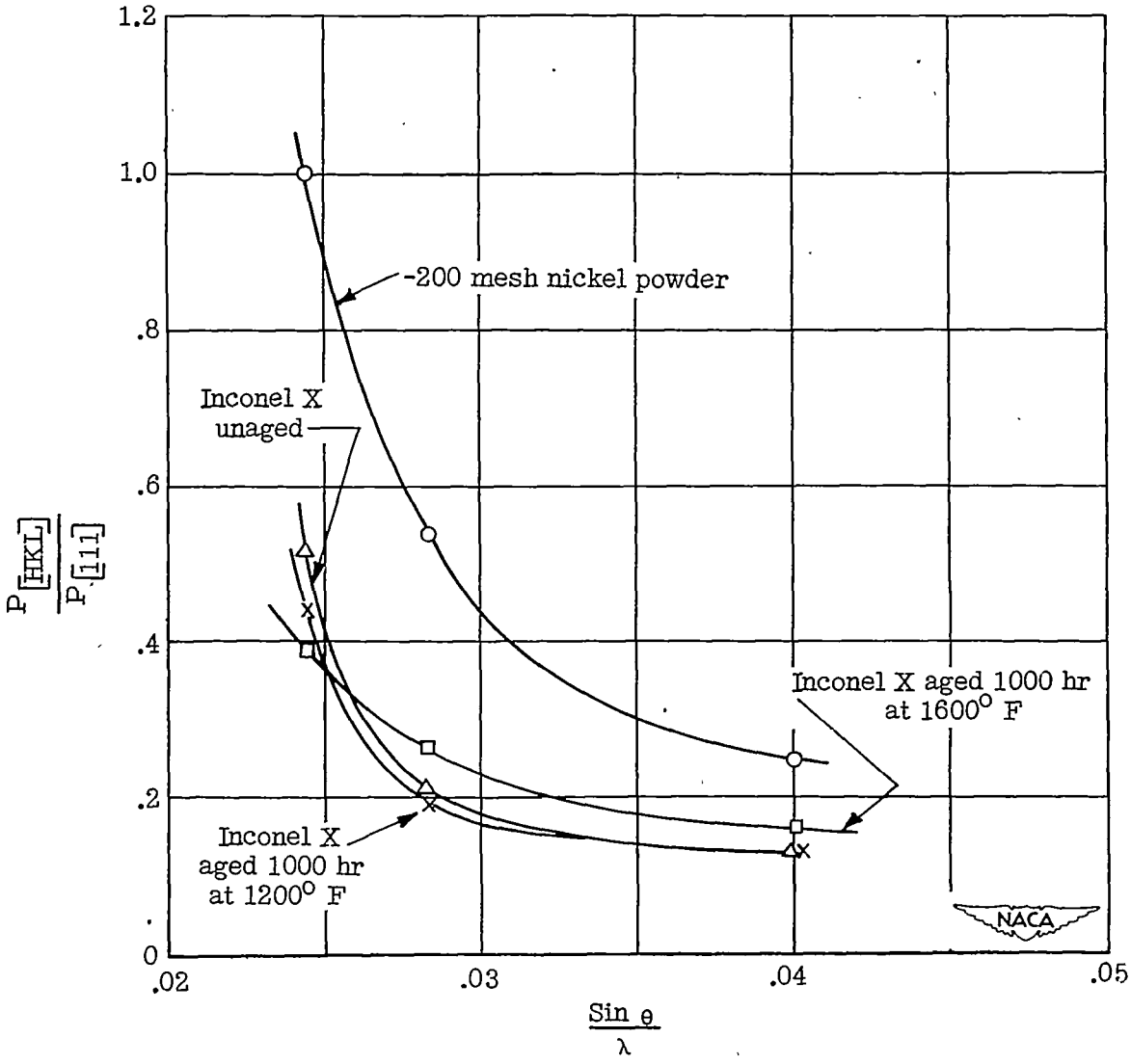


Figure 12.- Effect of aging on integrated intensities of [111], [200], and [220] lines of solution-treated Inconel X alloy. $P_{[HKL]}$, integrated intensity of indicated line; $P_{[111]}$, integrated intensity of nickel [111] line; $\theta$, Bragg angle; $\lambda$, wave length of X-radiation.

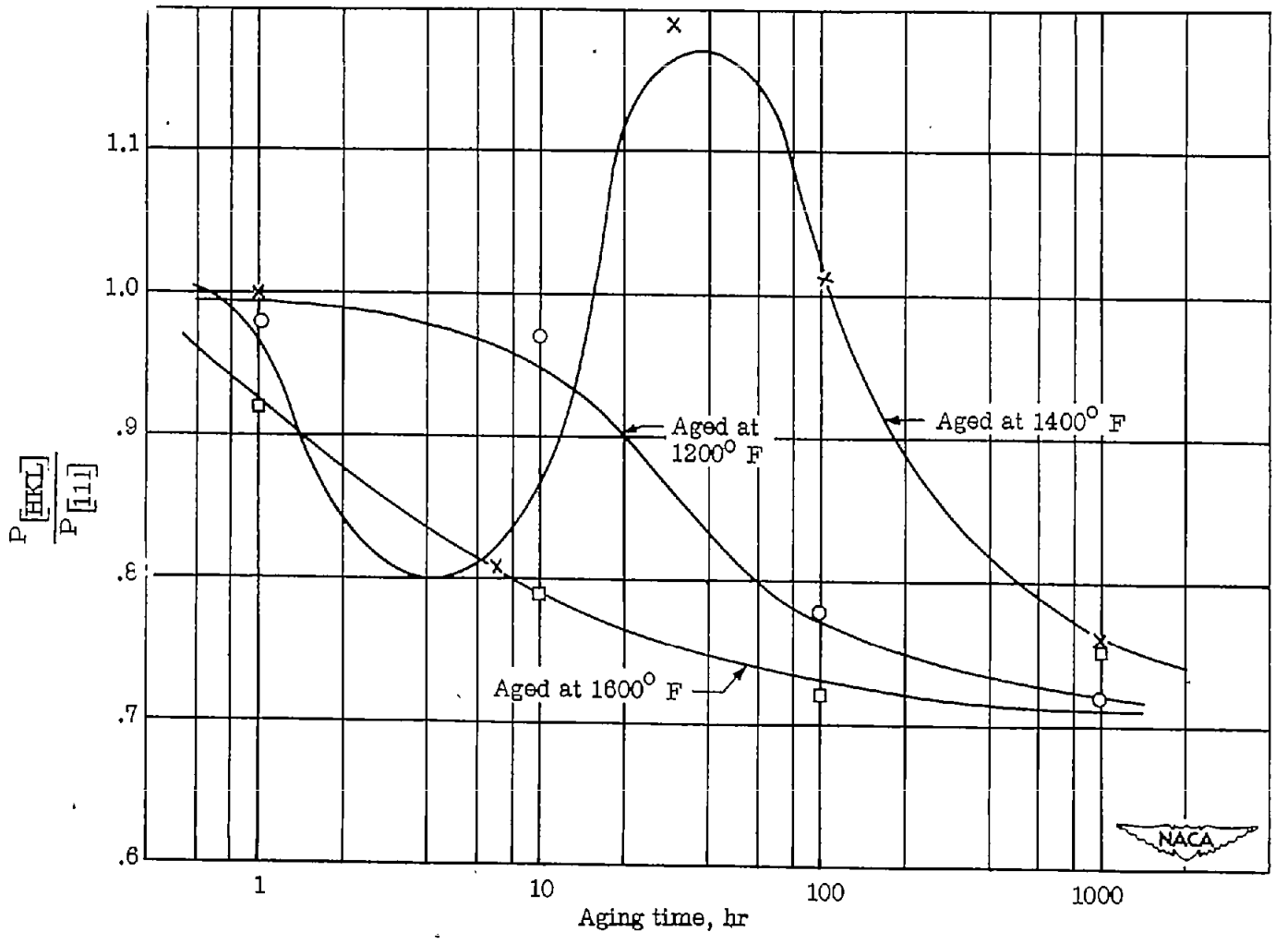


Figure 13.- Effect of aging on integrated intensity of [111] line of solution-treated Inconel X alloy. $P_{[HKL]}$, integrated intensity of indicated line; $P_{[111]}$, integrated intensity of [111] line of unaged material.

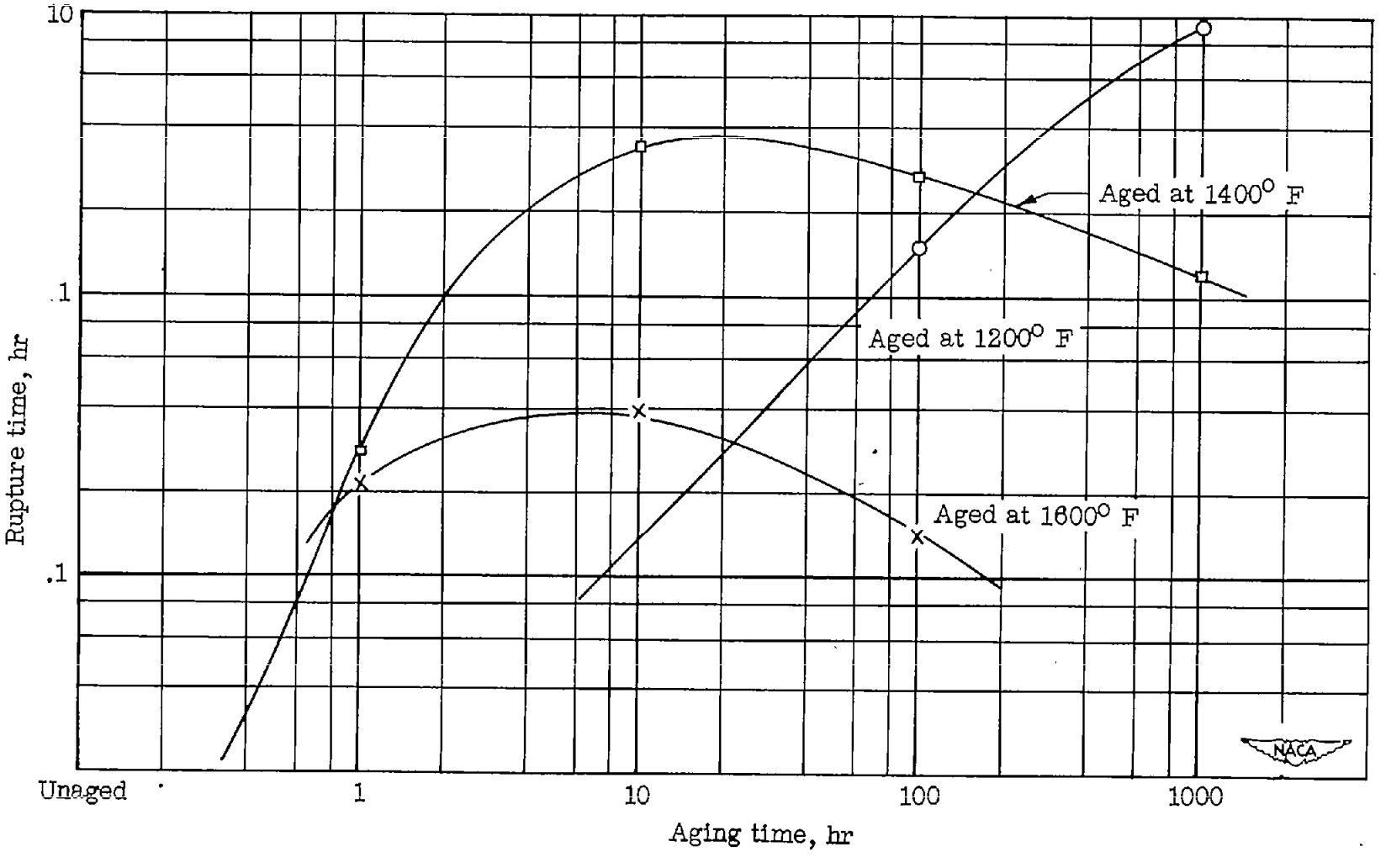


Figure 14.- Effect of aging on rupture time of solution-treated Inconel X alloy at 100,000 psi and 1200° F. Rupture time for unaged material was not measurable.

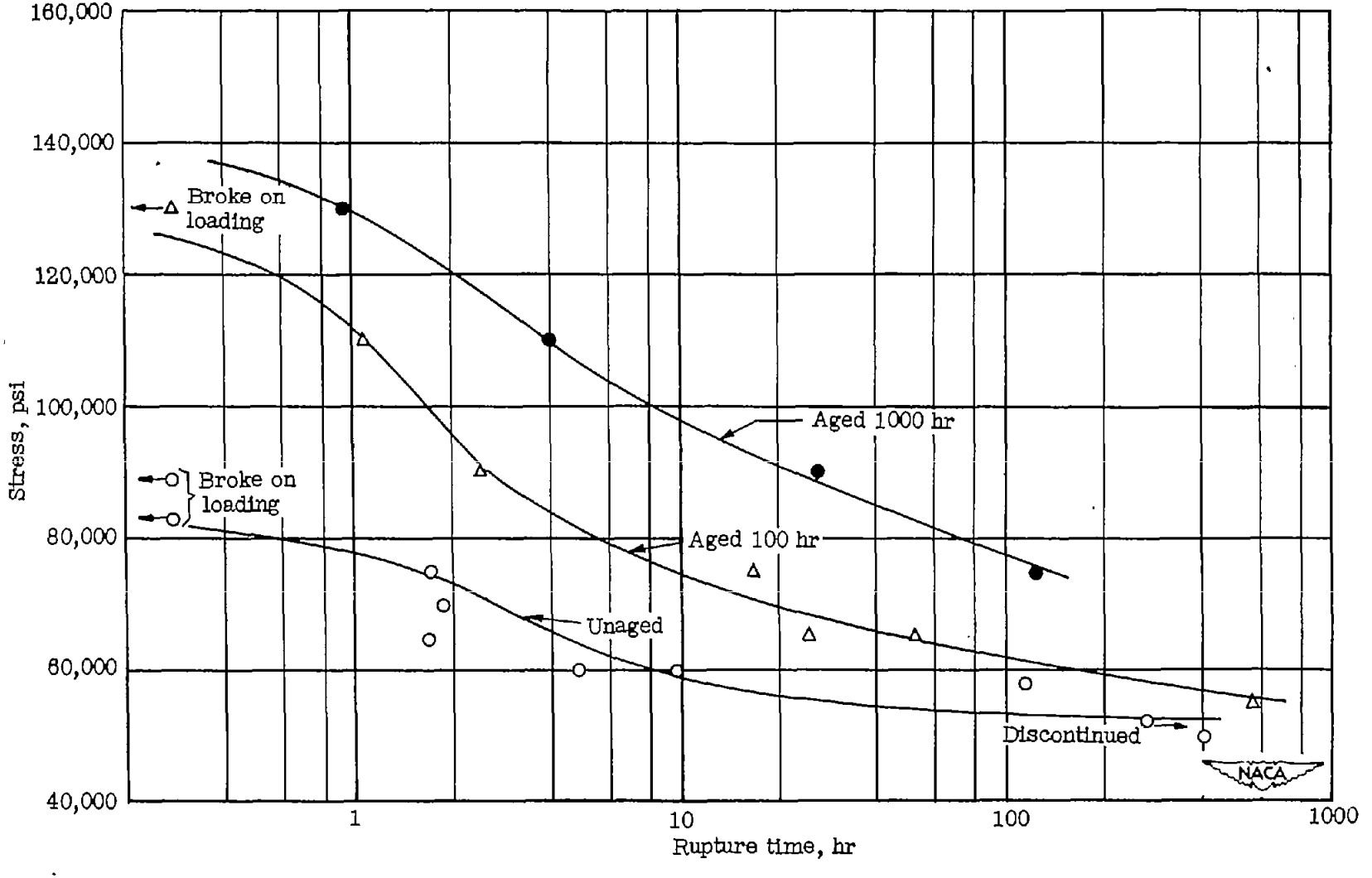


Figure 15.- Effect of aging at 1200° F on rupture characteristics of solution-treated Inconel X alloy at 1200° F.

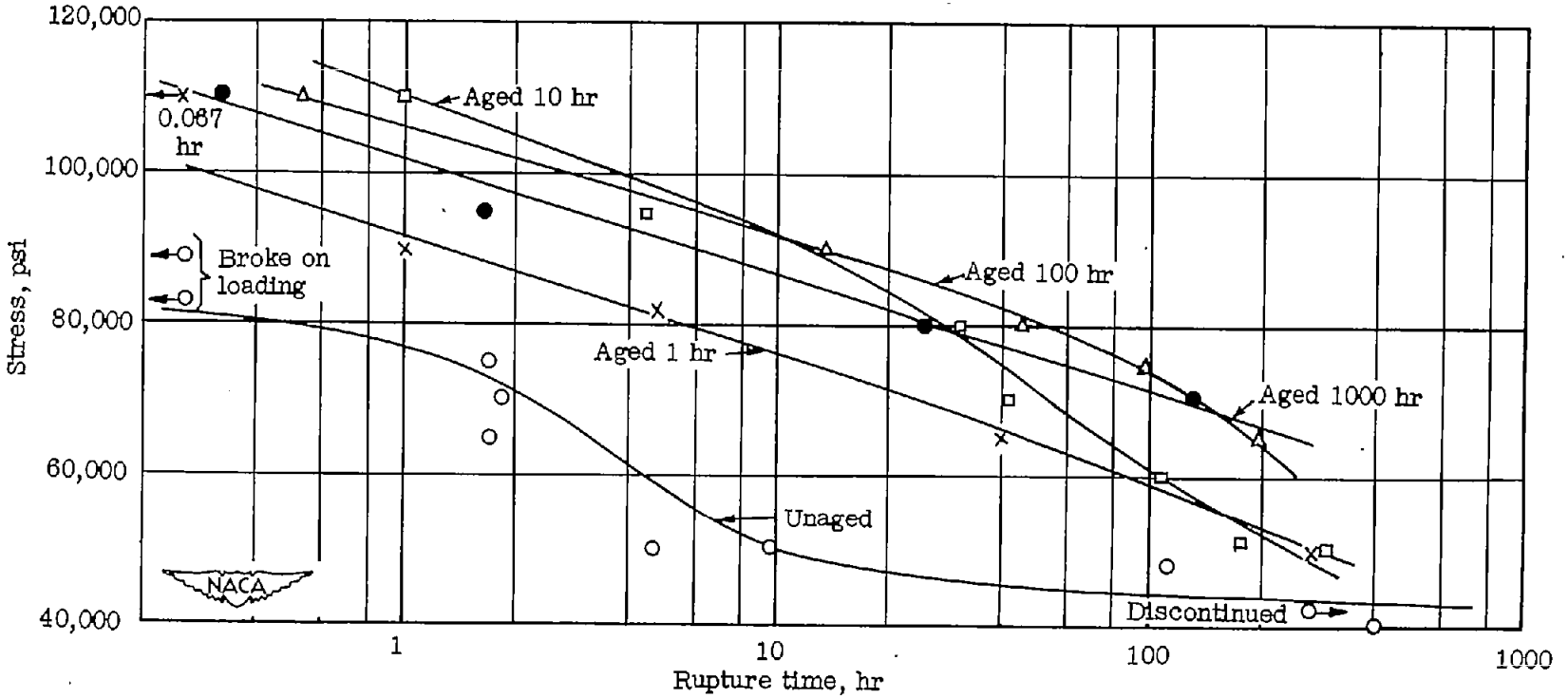


Figure 16.- Effect of aging at 1400° F on rupture characteristics of solution-treated Inconel X alloy at 1200° F.

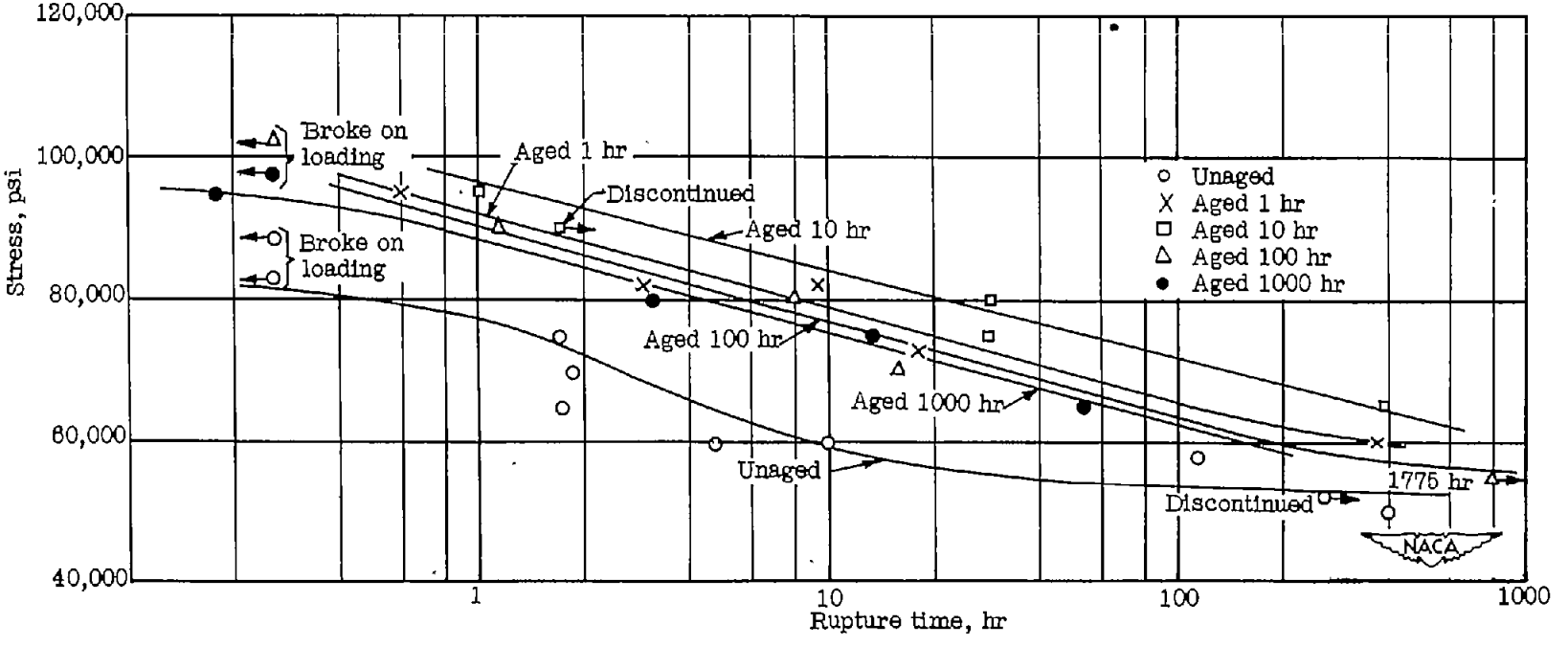


Figure 17.- Effect of aging at 1600° F on rupture characteristics of solution-treated Inconel X alloy at 1200° F.

(a) Unaged: failed in 1.7 hours under a stress of 75,000 psi.

(b) Unaged: failed in 112 hours under a stress of 58,000 psi.

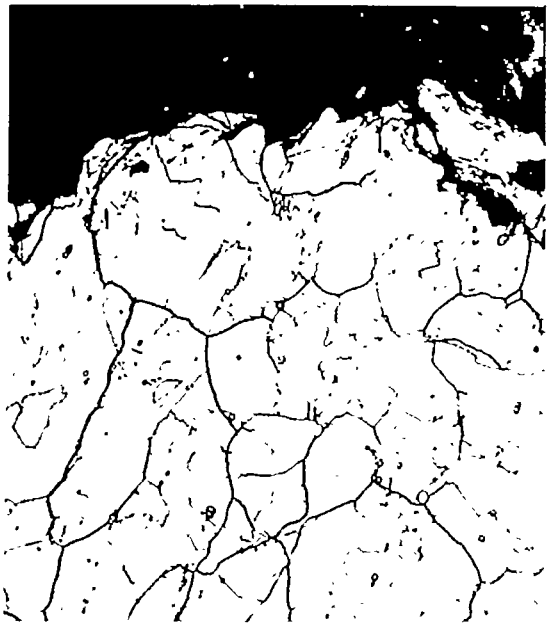

(c) Aged 1000 hours at 1200° F: failed in 0.95 hour under a stress of 130,000 psi.

(d) Aged 1000 hours at 1200° F: failed in 121 hours under a stress of 75,000 psi.

Figure 18.- Rupture characteristics at 1200° F of solution-treated and aged Inconel X alloy. Electrolytically etched in 10 percent oxalic acid. X100.

NACA

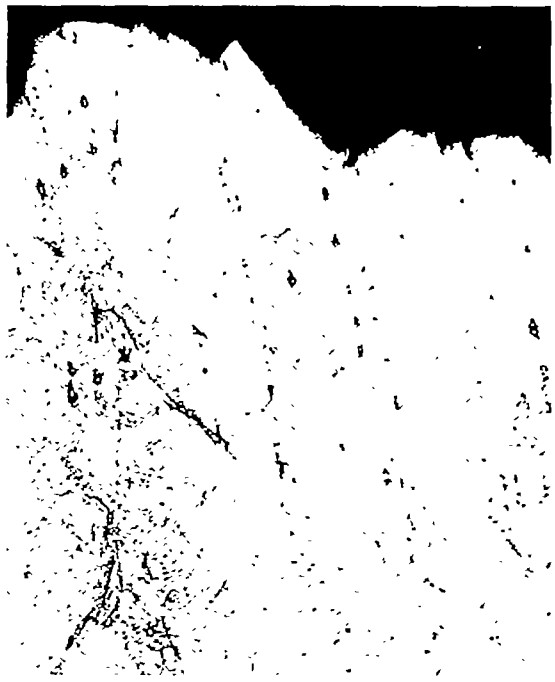

(e) Aged 1000 hours at 1600° F: failed in 3.17 hours under a stress of 80,000 psi.

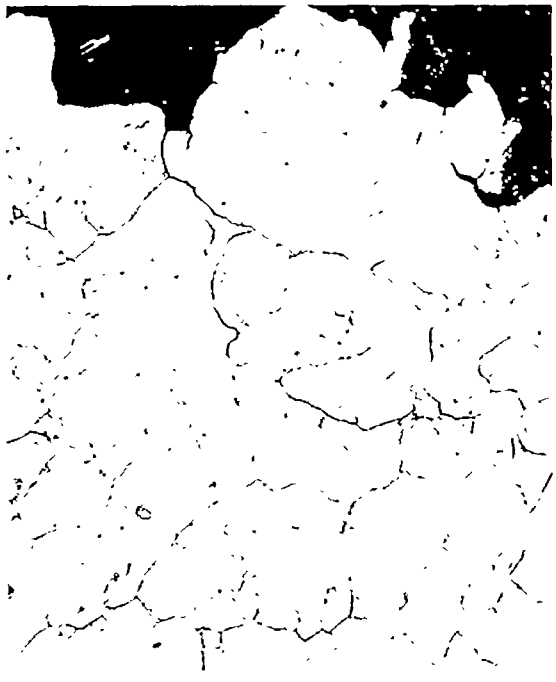

(f) Aged 1000 hours at 1600° F: failed in 53.5 hours under a stress of 65,000 psi.

Figure 18.- Concluded.

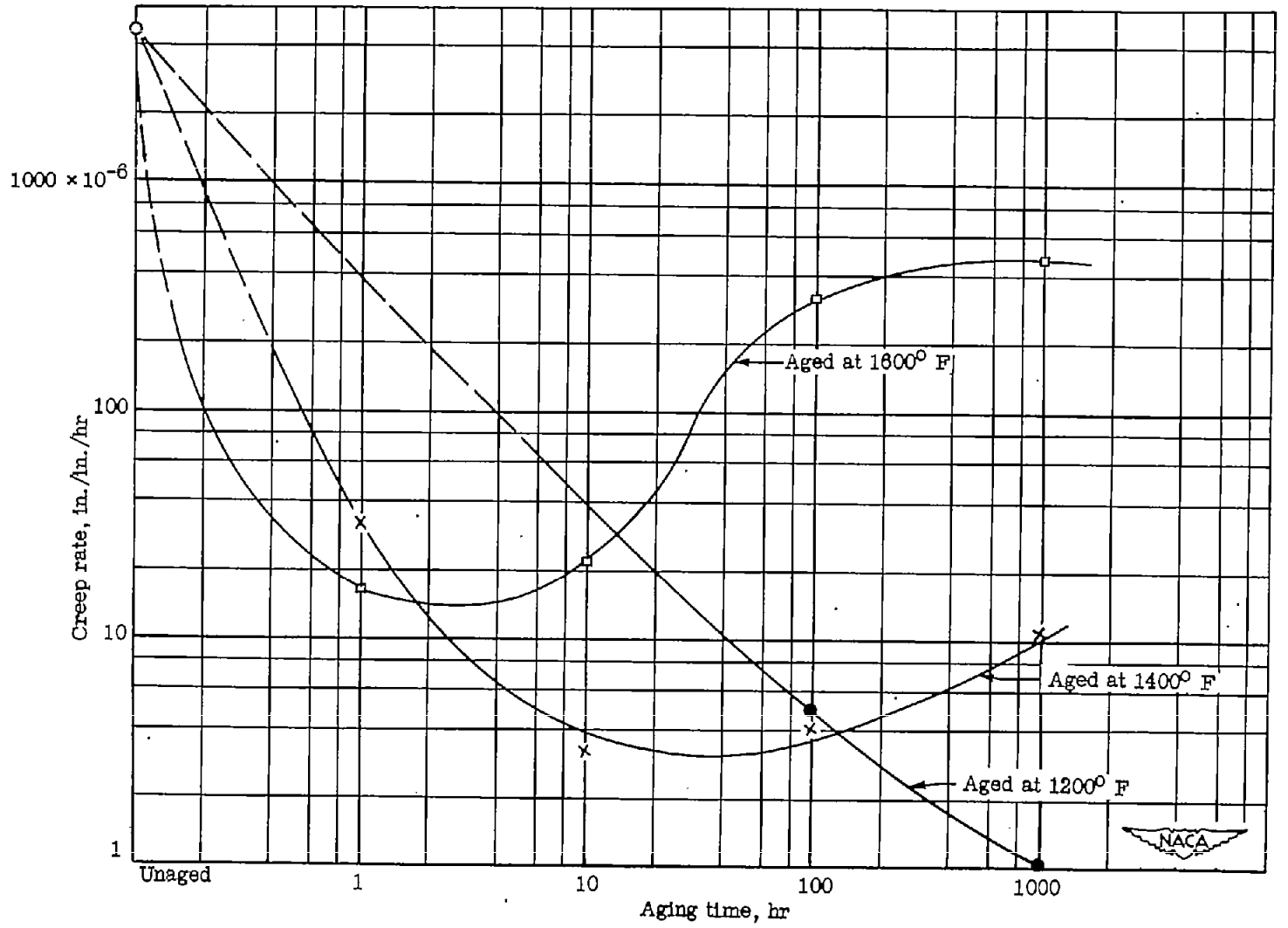


Figure 19.- Effect of aging on secondary creep rates of solution-treated Inconel X alloy at 65,000 psi and 1200° F.

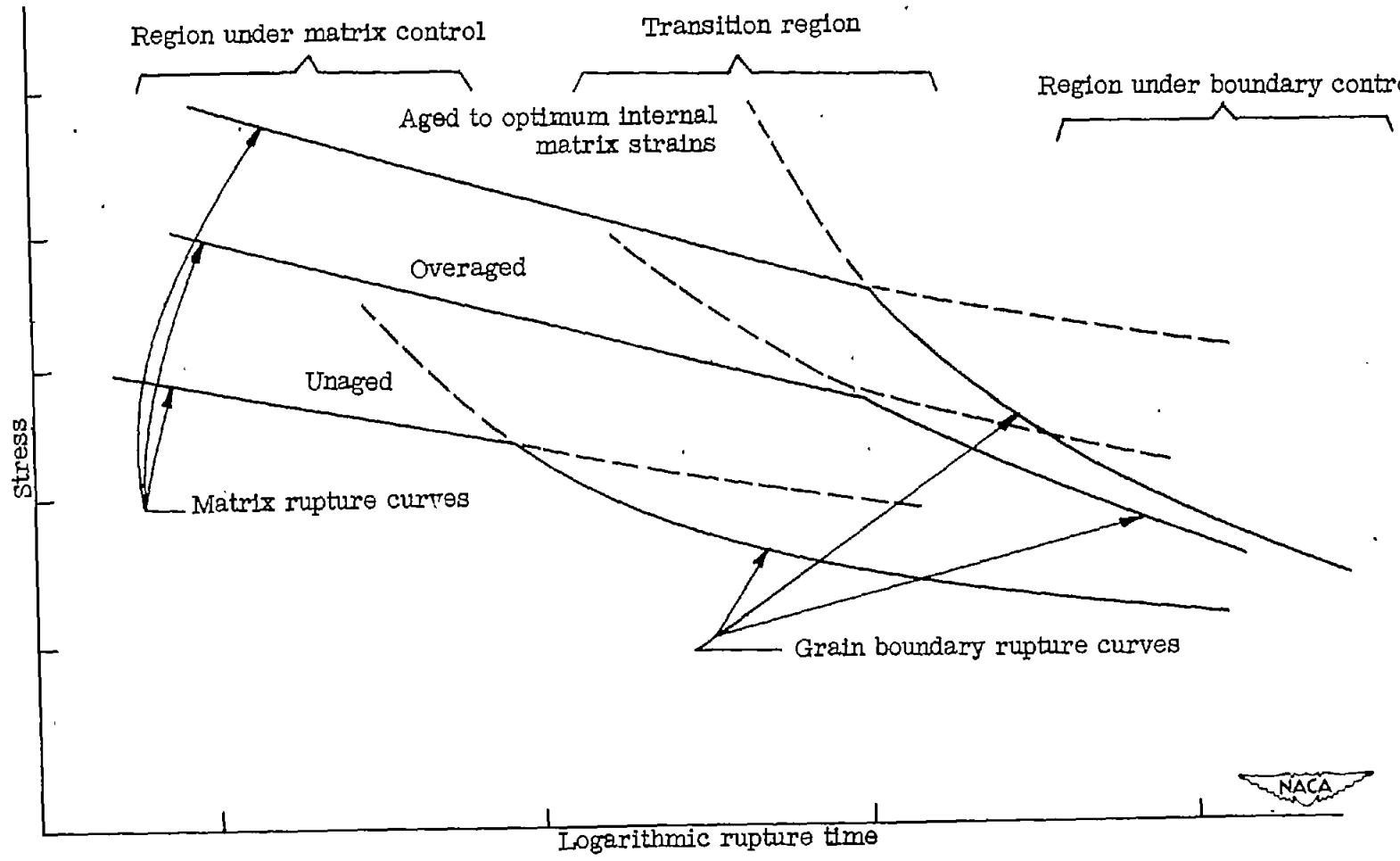


Figure 21.- Schematic diagram of rupture behavior of solution-treated and aged Inconel X alloy at 1200° F.

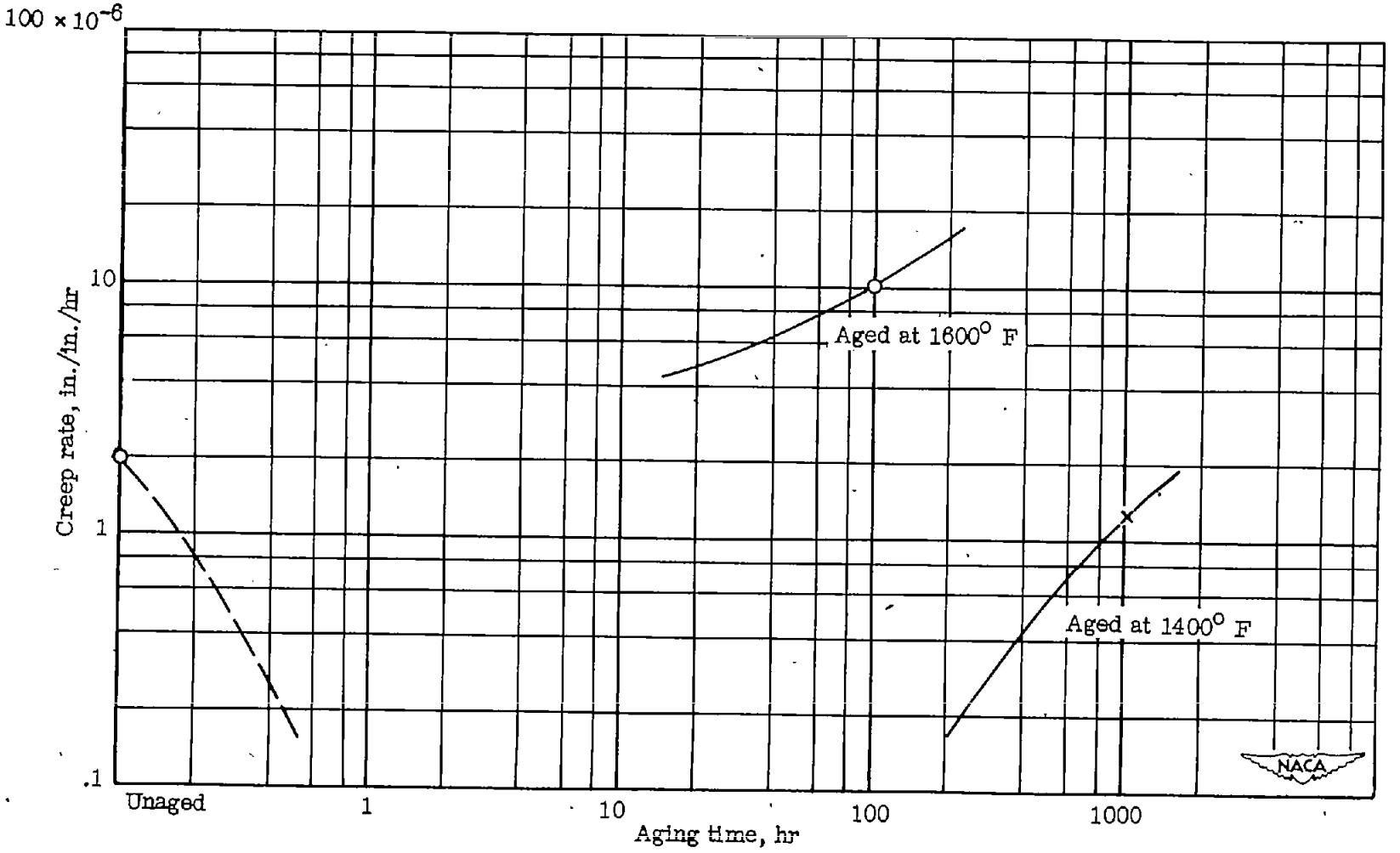


Figure 20.- Effect of aging on creep rates of solution-treated Inconel X alloy at 50,000 psi and 1200° F. Other creep rates for aging times of 1, 10, and 100 hours were not measurable.

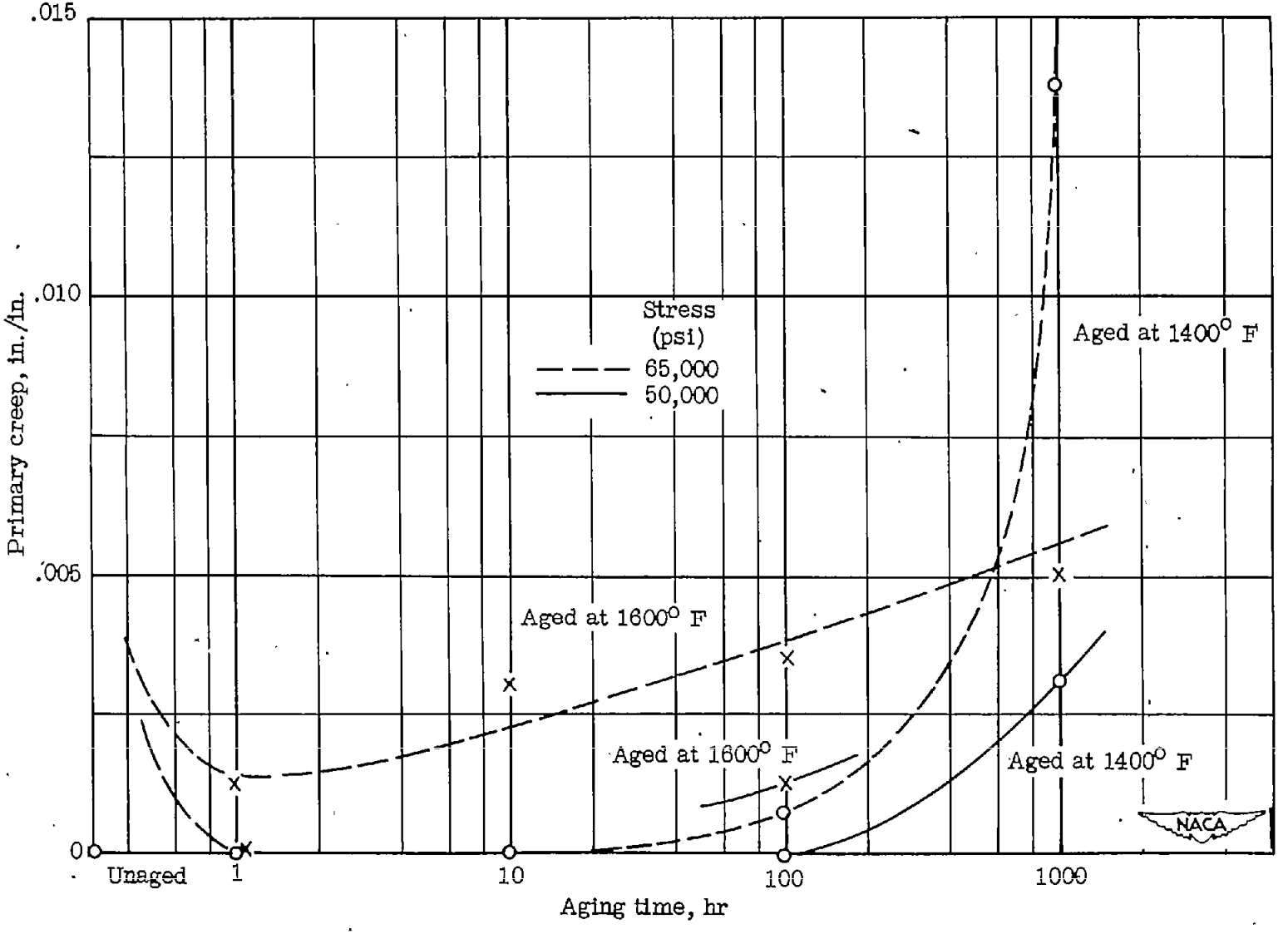


Figure 22.- Effect of aging on total primary creep of solution-treated Inconel X alloy at 1200° F.

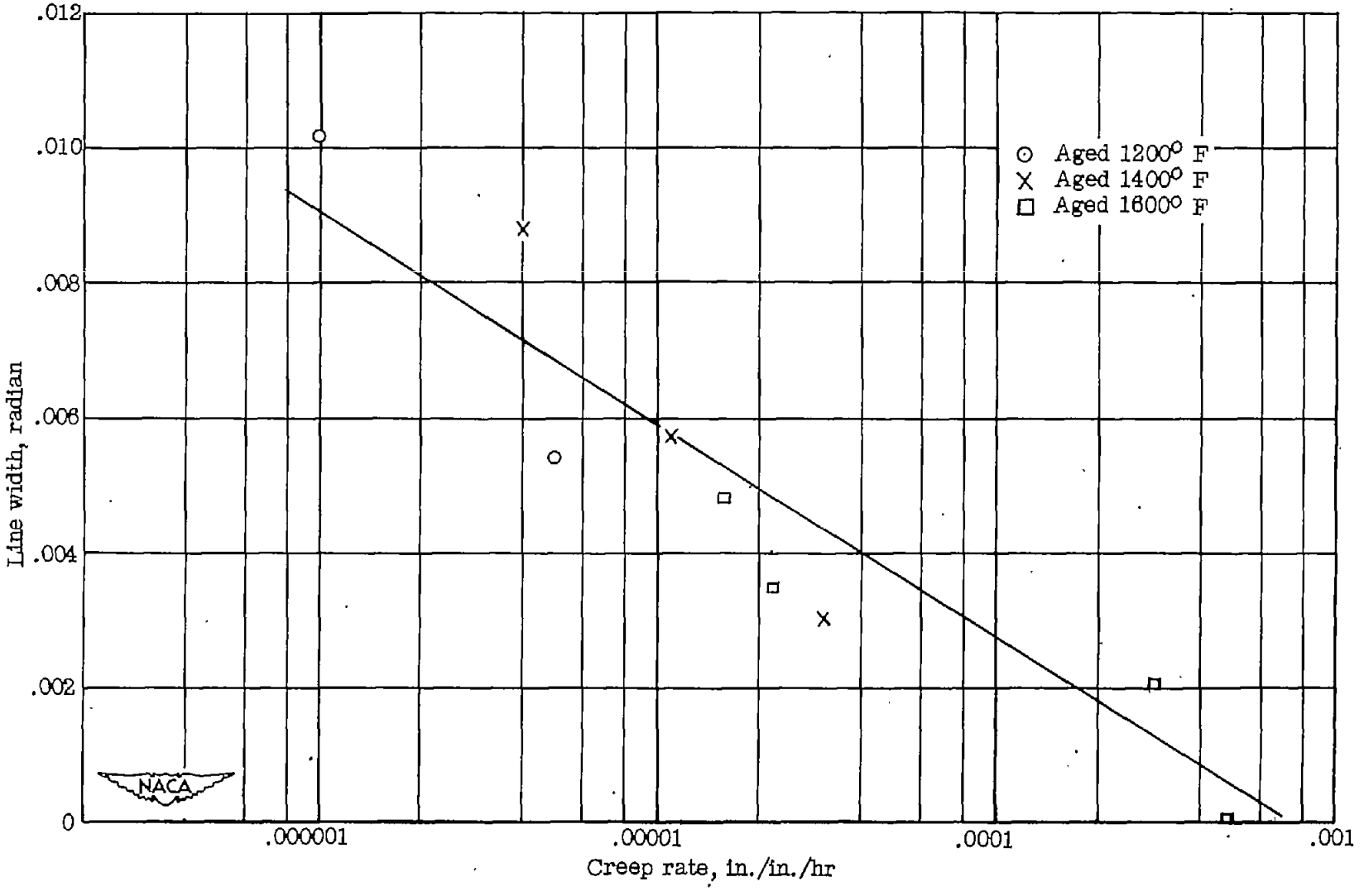


Figure 23.- Dependence of secondary creep rate upon mean internal strain of solution-treated and aged Inconel X alloy at 65,000 psi and 1200° F.

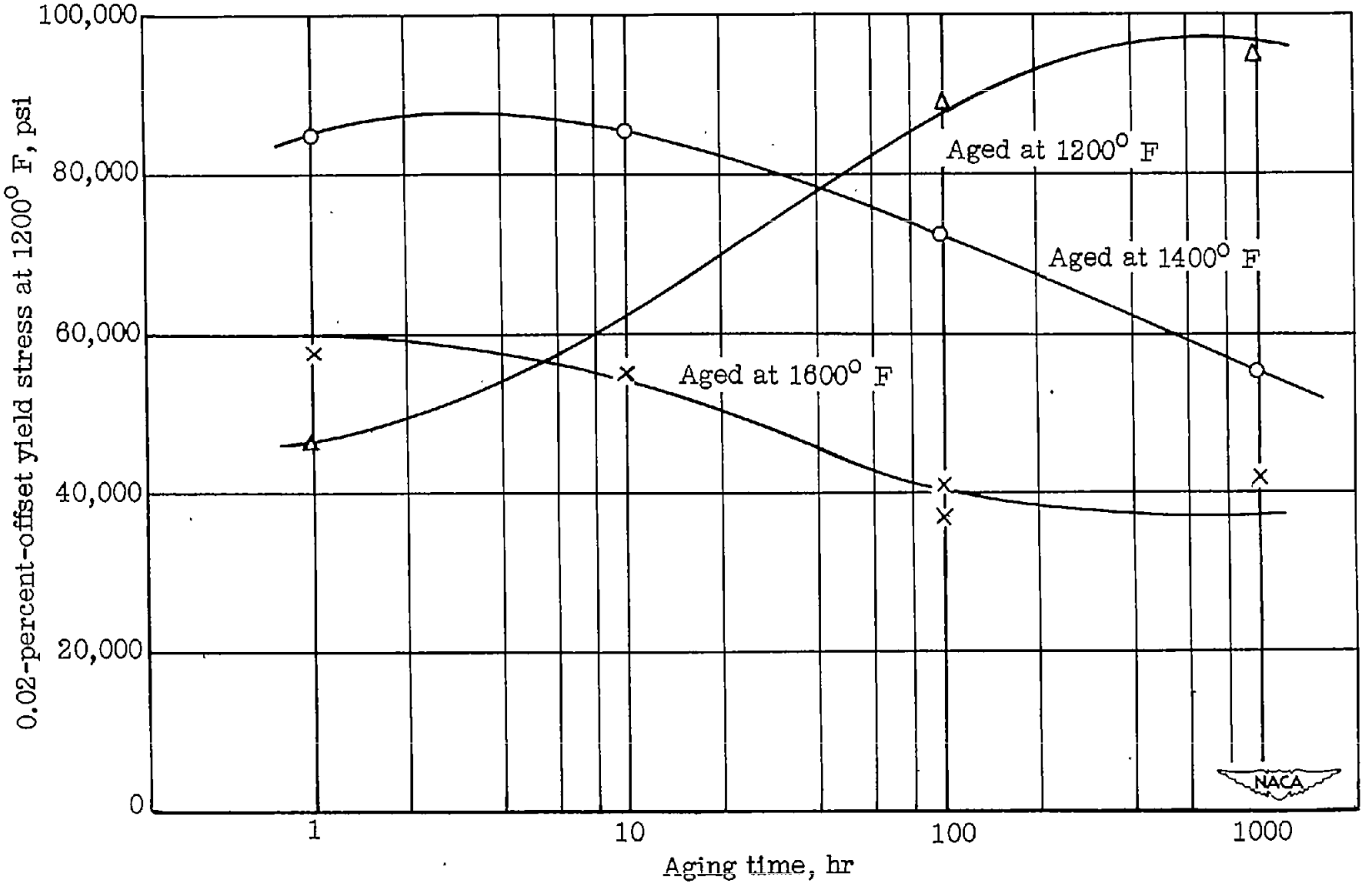


Figure 24.- Effect of aging on 0.02-percent-offset yield strength of solution-treated Inconel X alloy at 1200° F.

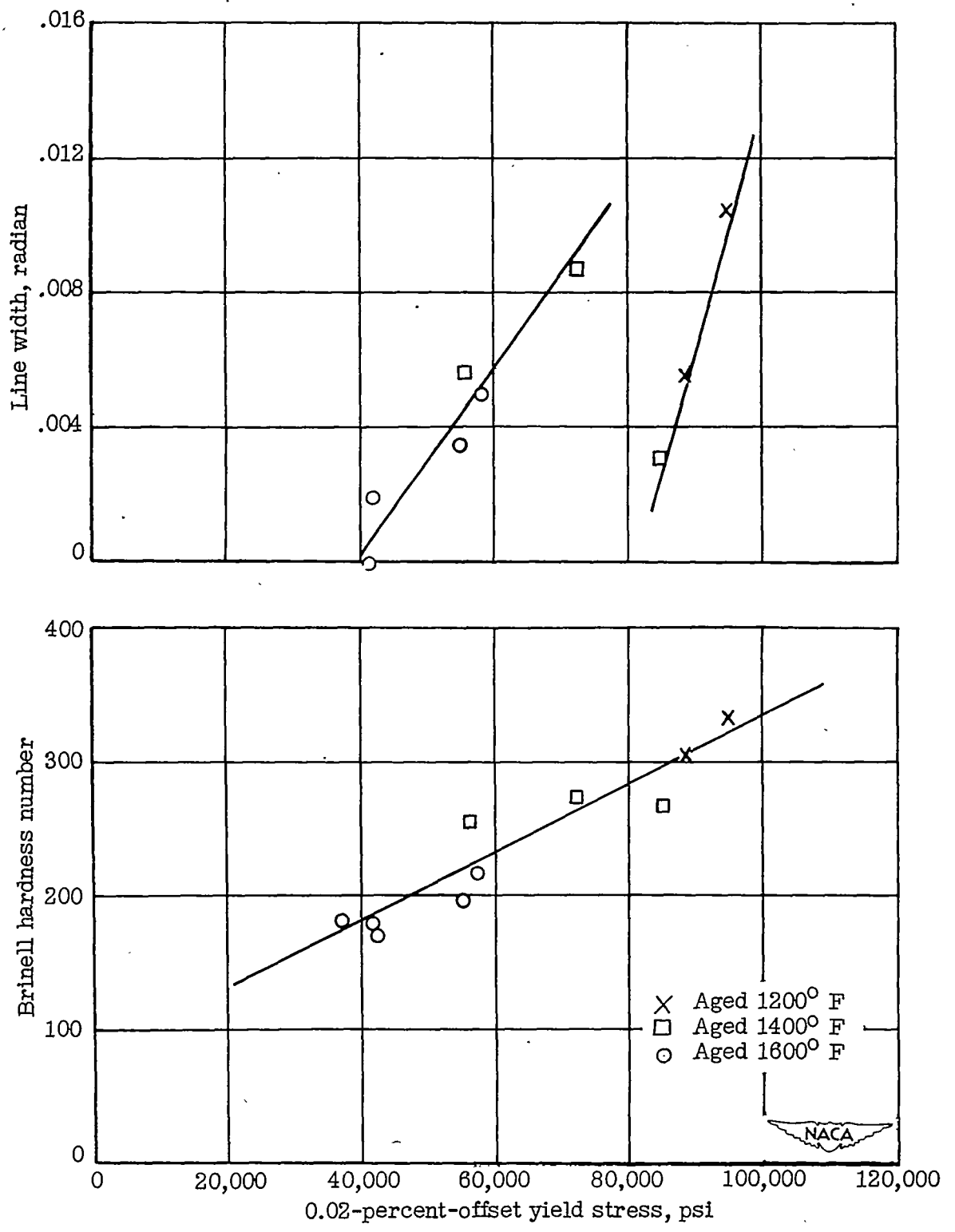


Figure 25.- Correlation of 0.02-percent-offset yield strength at 1200° F of solution-treated and aged Inconel X alloy with other physical properties.

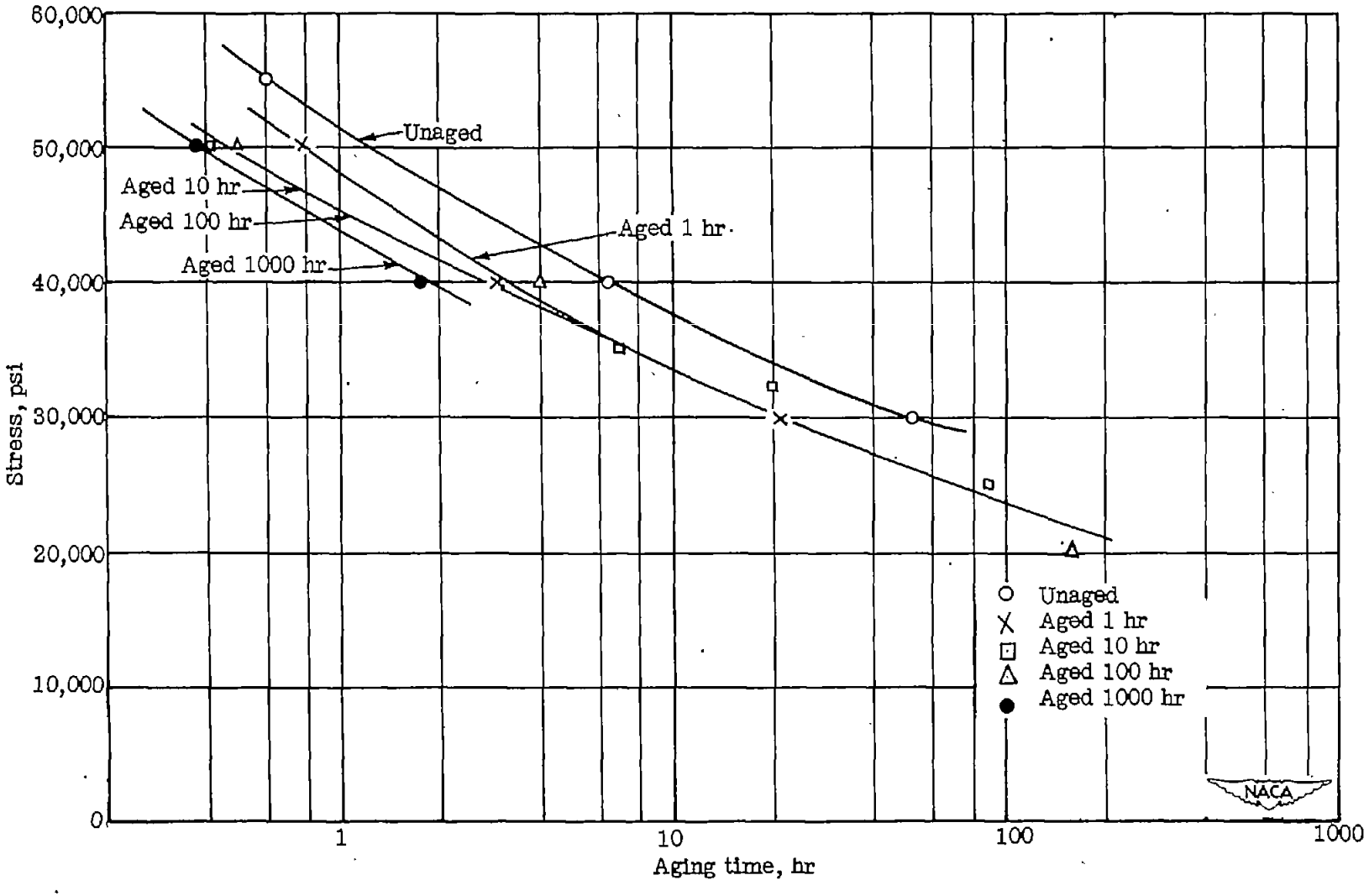


Figure 26.- Effect of aging at 1600° F on rupture strength of solution-treated Inconel X alloy at 1500° F.

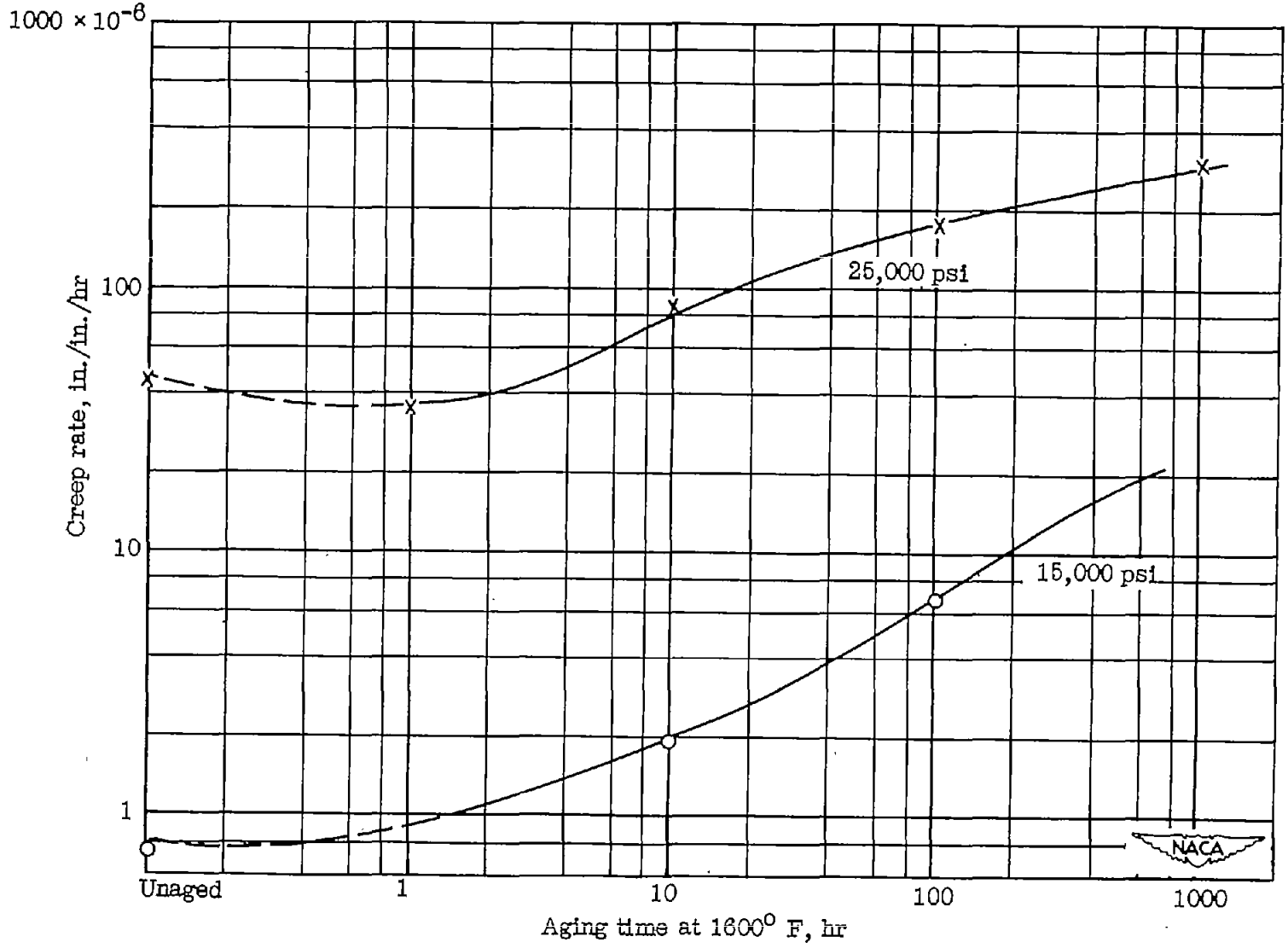


Figure 27.- Effect of aging at 1600° F on creep rates of solution-treated Inconel X alloy at 1500° F.

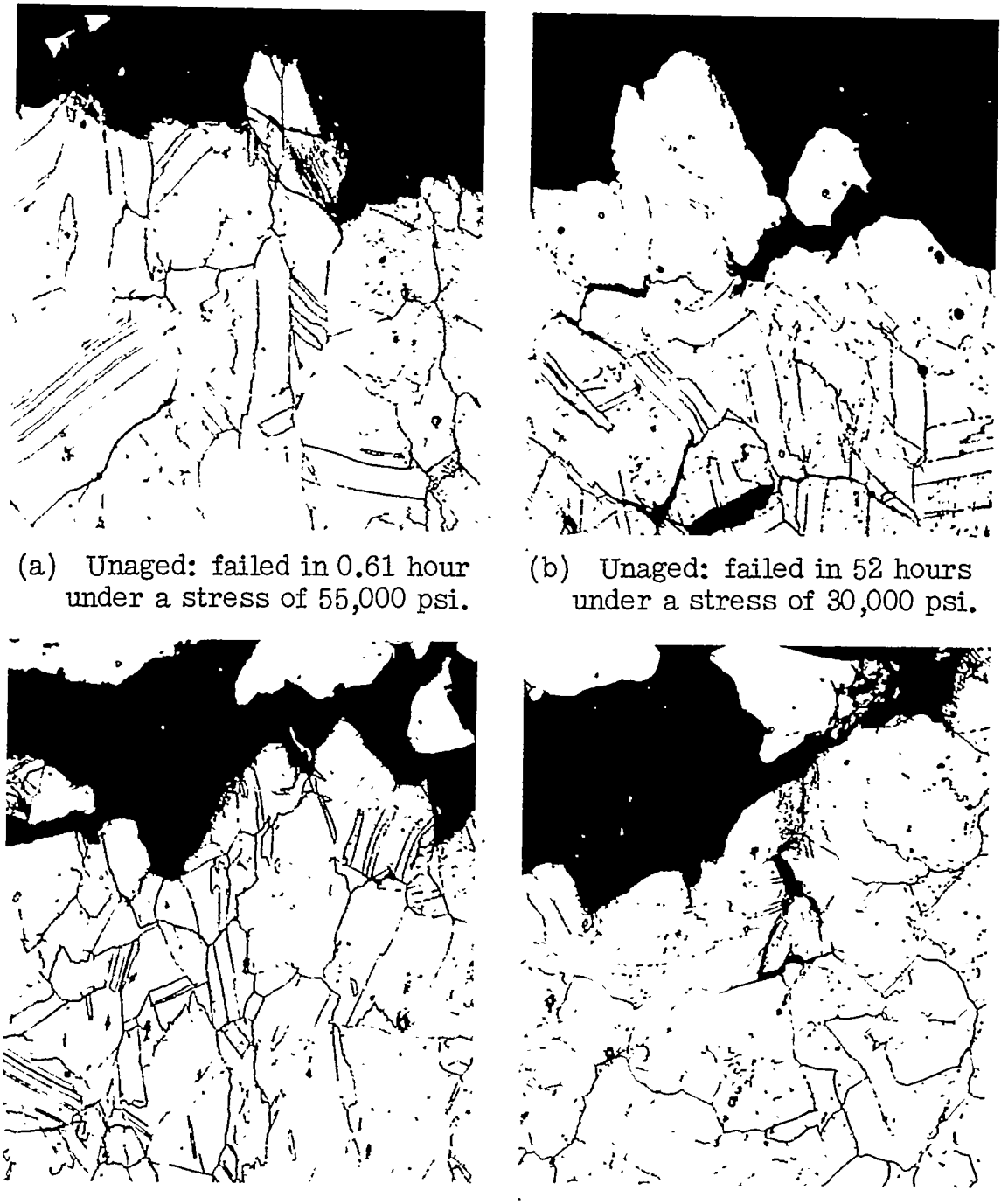

(a) Unaged: failed in 0.61 hour under a stress of 55,000 psi.

(b) Unaged: failed in 52 hours under a stress of 30,000 psi.

(c) Aged 100 hours at 1600° F: failed in 0.51 hour under a stress of 50,000 psi.

(d) Aged 100 hours at 1600° F: failed in 156 hours under a stress of 20,000 psi.

Figure 28.- Rupture characteristics at 1500° F of solution-treated and aged Inconel X alloy. Electrolytically etched in 10 percent oxalic acid. X100.

NACA

21

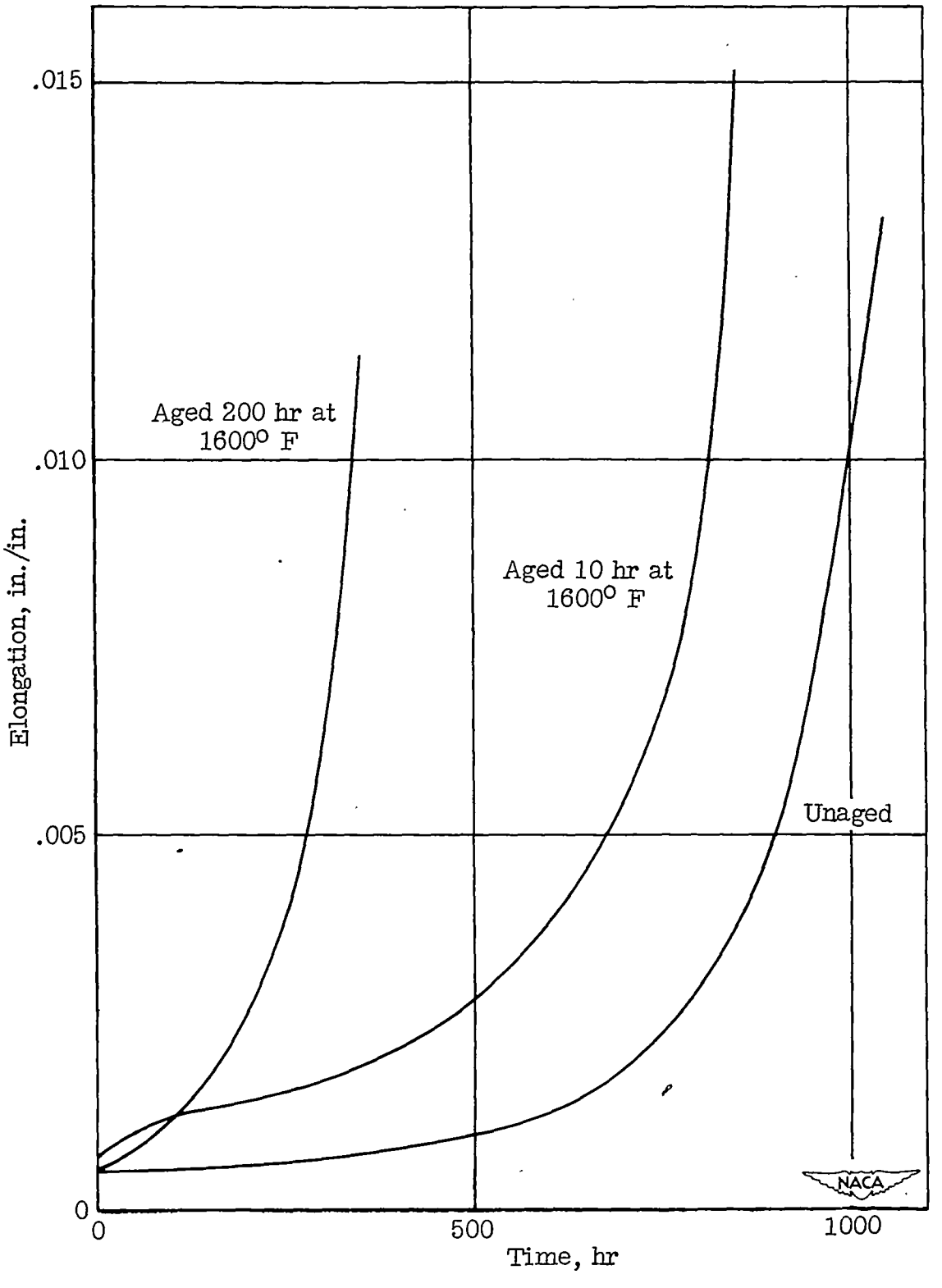


Figure 29.- Typical creep curves at 1500° F and 15,000 psi for solution-treated and aged Inconel X alloy.

NACA-Langley - 6-7-51 - 1000